

# Federated Echo State Learning for Minimizing Breaks in Presence in Wireless Virtual Reality Networks

Mingzhe Chen\*, Omid Semiari<sup>‡</sup>, Walid Saad<sup>†</sup>, Xuanlin Liu\*, and Changchuan Yin\*

\*Beijing Key Laboratory of Network System Architecture and Convergence,  
Beijing University of Posts and Telecommunications, Beijing, China,  
Emails: chenmingzhe@bupt.edu.cn and ccyin@ieee.org.

<sup>‡</sup>Department of Electrical and Computer Engineering, Georgia Southern University, Statesboro, GA, USA,  
Email: osemiari@georgiasouthern.edu.

<sup>†</sup>Wireless@VT, Bradley Department of Electrical and Computer Engineering, Virginia Tech, Blacksburg, VA, USA, Email: walids@vt.edu.

## Abstract

In this paper, the problem of enhancing the virtual reality (VR) experience for wireless users is investigated by minimizing the occurrence of breaks in presence (BIPs) that can detach the users from their virtual world. To measure the BIPs for wireless VR users, a novel model that jointly considers the VR applications, transmission delay, VR video quality, and users' awareness of the virtual environment is proposed. In the developed model, the base stations (BSs) transmit VR videos to the wireless VR users using directional transmission links so as to increase the data rate of VR users, thus, reducing the number of BIPs for each user. Therefore, the mobility and orientation of VR users must be considered when minimizing BIPs, since the body movements of a VR user may result in blockage of its wireless link. The BIP problem is formulated as an optimization problem which jointly considers the predictions of users' mobility patterns, orientations, and their BS association. To predict the orientation and mobility patterns of VR users, a distributed learning algorithm based on the machine learning framework of deep echo state networks (ESNs) is proposed. The proposed algorithm uses concept from *federated learning* to enable multiple BSs to locally train their deep ESNs using their collected data and cooperatively build a learning model to predict the entire users' mobility patterns and orientations. Using these predictions, the user association policy that minimizes BIPs is derived. Simulation results demonstrate that the developed algorithm reduces the users' BIPs by up to 16% and 26% gains, respectively, compared to centralized ESN and deep learning algorithms.

*Index Terms*— BIP; VR; deep echo state networks; federated learning.

## I. INTRODUCTION

Deploying virtual reality (VR) applications over wireless networks is an essential stepping stone towards flexible deployment of pervasive VR applications [1]. However, to enable a seamless and immersive wireless VR experience, it is necessary to introduce novel wireless networking solutions that can meet stringent quality-of-service (QoS) requirements of VR applications in terms of delivering high data rates and low latency [2]. In wireless VR networks, the sudden data rate reductions or large delay can negatively impact the users' VR experience (e.g., due to interruptions in VR video streams). Due to such an interruption in the virtual world, VR users will experience *breaks in presence (BIPs)* events that can be detrimental to their immersive VR experience. While the fifth-generation (5G) new radio supports operation at high frequency bands (with abundant bandwidth) as well as flexible frame structure to minimize latency, performance of communication links at high frequencies is highly prone to blockage. That is, if an object blocks the wireless link between the BS and a VR user, the data rate can drop significantly and lead to a BIP. In addition to wireless factors such as delay and data rate, behavioral metrics related to each VR user such as the user's *awareness* can also affect BIPs. Here, awareness is defined as each wireless VR user's perceptions and actions in its individual VR environment. For instance, a user might be too sensitive to slight variations in VR video quality changes, while another user might be more tolerant. Therefore, to minimize the BIPs of VR users, it is necessary to jointly consider all of the wireless environment and user-specific metrics that cause BIPs, such as link blockage, user mobility, user orientation, user association, and user awareness.

Recently, several works have studied a number of problems related to wireless VR networks [1], [3]–[9]. The work in [1] provides a comprehensive survey of challenges and opportunities for deploying VR devices over wireless networks. In [3], the authors develop a framework for mobile VR delivery by leveraging caching and computing capabilities of mobile VR devices in order to alleviate the traffic burden over wireless networks. The authors in [4] study the problem of supporting visual and haptic perceptions over wireless cellular networks. A communications-constrained mobile edge computing framework is proposed in [5] to reduce wireless resource consumption. The work in [6] proposes a concrete measure for the delay perception of VR users. The authors in [7] present a scheme of proactive computing and high-frequency, millimeter

wave (mmWave) transmission for wireless VR networks. In [8], the authors design several experiments for quantifying the performance of tile-based 360° video streaming over a real cellular network. Our previous works in [9] studied the problems of resource allocation and 360° content transmission for wireless VR users. However, most of these existing works do not provide a comprehensive BIP model that accounts for the transmission delay, the quality of VR videos, VR applications, and user awareness. Moreover, the prior art in [1], [3]–[9] does not jointly consider the impact of the users’ body movements when using mmWave communications with highly directional links to support high data rates for VR video transmissions.

To address this challenge, machine learning techniques can be used to predict the users’ movements and proactively determine the user associations that can minimize BIPs. The use of machine learning algorithms for predicting the users’ movement in wireless networks was studied in [10]–[16]. However, these works focus on scenarios where users are not mobile, and hence, user association does not change with time. Hence, the data for each VR user’s movement can be collected by its associated BS. However, in real mobile VR scenarios, users will move and change their association and the data related to the users’ movement is dispersed across multiple BSs. The BSs may not be able to transmit all of their collected data pertaining users’ movements to each other, due to the high overhead of data transmission. Moreover, sending all the information to a centralized processing server will cause very large latencies that cannot be tolerated by VR applications. Thus, centralized machine learning algorithms will not be useful to predict real-time movements of the VR users. To this end, *a distributed learning framework that can be trained by the collected data at each BS and cooperatively build a learning model that can predict the entire users’ mobility and orientations is needed.*

The main contribution of this paper is a novel framework for minimizing BIPs within VR applications that operate over wireless cellular networks. To our best knowledge, *this is the first work that analyzes how a wireless network with distributed learning can minimize BIP for VR users and enhance their virtual world experience.* The key contributions therefore include:

- For wireless VR users, we mathematically model the BIP that jointly considers VR applications, the delay of VR video and tracking information transmission, VR video quality, and the users’ awareness.
- To minimize the BIP of wireless VR users, we develop a federated echo state network (ESN) [17] learning algorithm that enables BSs to locally train their machine learning algorithms

using the data collected from the users' locations and orientations. Then, the BSs can cooperatively build a learning model by sharing their trained models to predict the users' mobility patterns and orientations. Based on these predictions, we perform fundamental analysis to find an efficient user association for each VR user that minimizes the BIPs.

- To analyze the prediction accuracy of the federated ESN learning algorithm, we study the memory capacity of federated ESNs. The memory capacity characterizes the ability of the ESN model to record historical locations and orientations of each VR user. As the memory capacity increases, the prediction accuracy will increase and, hence, BSs can find users' association that will minimize the number of BIPs. The analytical results show that the memory capacity of the ESN depends on the number of neurons in each ESN model and the values of matrices that are used to generate the ESN model.
- Simulation results demonstrate that our proposed algorithm can achieve, respectively, 16% and 26% gains in terms of total BIPs compared to the centralized ESN and deep learning algorithm in [13]. The results also show that the proposed algorithm improves the cumulative distribution function (CDF) of up to 38% and 71% gains at a BIP of 15 compared to the centralized ESN and deep learning algorithms, respectively.

The rest of this paper is organized as follows. The problem formulation is presented in Section II. The federated ESN learning algorithm for the predictions is proposed in Section III. In Section IV, the memory capacity of various ESN models are analyzed. The user association is found in Section V. In Section VI, numerical simulation results are presented and conclusions are drawn in Section VII.

## II. SYSTEM MODEL AND PROBLEM FORMULATION

Consider a cellular network that consists of a set  $\mathcal{B}$  of  $B$  BSs that service a set  $\mathcal{U}$  of  $U$  VR users. In this model, BSs act as VR controllers that can collect the tracking information related to the users' movements via VR sensors and use the collected data to generate the VR videos for their associated users. In particular, the uplink is used to transmit tracking information such as users' locations and orientations from the VR devices to the BSs, while the downlink is used to transmit VR videos from BSs to VR users. For user association, the VR users can associate with different BSs for uplink and downlink data transmissions. We consider practical scenarios when the type of VR application can depend on the location of the user. For example, a given

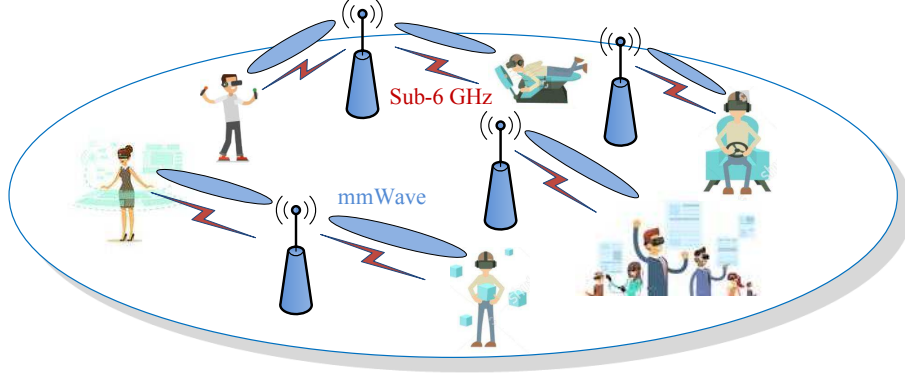


Fig. 1. The architecture of a wireless VR network. In this architecture, the Sub-6 GHz uplink is used to transmit tracking information and the mmWave downlink is used to transmit VR videos.

TABLE I  
LIST OF NOTATIONS

Notation	Description	Notation	Description
$U$	Number of VR users	$x_{it}, y_{it}$	Location of user $i$ at time $t$
$B$	Number of BSs	$F^{\text{UL}}$	Total uplink bandwidth of each BS
$P_u$	Transmit power of each user	$Y$	Number of locations and orientations that each ESN can predict
$d_{ij}$	Distance between BS $j$ and user $i$	$U_j^{\text{UL}}$	Number of uplink users associated with BS $j$
$F^{\text{DL}}$	Bandwidth of each beam	$\mathcal{U}_j$	Set of the users associated with BS $j$
$\mathcal{U}$	Set of VR users	$\rho^2$	Power of the Gaussian noise
$\mathcal{B}$	Set of BSs	$G_{ij}$	Antenna gain of the link from BS $j$ to user $i$
$V$	Number of beams of each BS	$b_i(\chi_{it})$	Blockage effect caused by user $i$
$\mathbf{x}_{ij}$	Input of each ESN	$c_{ij}^{\text{DL}}$	Downlink data rate of user $i$
$P_{it}$	Total BIP of each user $i$	$\chi_{it}$	Orientation of user $i$ at time $t$
$N_W$	Number of neurons in ESN	$n_{ijt}$	Number of users located between user $i$ and BS $j$
$G_A$	Game mode	$h_{ij}^{\text{LoS}}$	LoS link between user $i$ and BS $j$
$\mathbf{y}_{ij,t}$	Output of each ESN	$h_{ij}^{\text{NLoS}}$	NLoS link between user $i$ and BS $j$
$c_{ij}^{\text{UL}}$	Uplink data rate of user $i$	$P_{it}^{\text{W}}$	BIP of user $i$ caused by data transmission

user that works in a lab may use certain VR applications for training or research purposes, while using the VR device for entertainment at home. This information will be used by BSs to predict users' locations and orientations and proactively determine efficient user associations. Table II summarizes our notations.

#### A. Transmission Model

We consider both uplink and downlink transmission links between BSs and VR users. The VR users can operate at both mmWave and sub-6 GHz frequencies [18]. The VR videos are

transmitted from BSs to VR users over the 28 GHz band. Meanwhile, the tracking information is transmitted from VR devices to their associated BSs over a sub-6 GHz frequency band. This is due to the fact that sub-6 GHz frequencies with limited bandwidth cannot support the large data rates required for VR video transmissions. However, it can provide reliable communications for sending small data sized users' tracking information. Next, we first introduce the transmission of the users' tracking information in the uplink. Then, we specify the VR video transmission via downlink mmWave links.

1) *Uplink Transmissions of User Tracking Information:* Let  $(x_{it}, y_{it})$  be the Cartesian coordinates for the location of user  $i$  at time  $t$  and  $S$  be the data size of each user's tracking information, including location and orientation.  $S$  depends on the VR system (i.e., HTC Vive [19] or Oculus [20]). The data rate for transmitting the tracking information from VR user  $i$  to BS  $j$  is given by:

$$c_{ij}^{\text{UL}}(x_{it}, y_{it}) = \frac{F^{\text{UL}}}{U_j^{\text{UL}}} \log_2 \left( 1 + \frac{P_u g_{ij} d_{ij}^{-\beta}(x_{it}, y_{it})}{\sum_{k \in \mathcal{U}, k \neq i} P_u g_{kj} d_{kj}^{-\beta}(x_{kt}, y_{kt}) + \rho^2} \right), \quad (1)$$

where  $F^{\text{UL}}$  is the total uplink bandwidth of each BS  $j$  which is assumed to be equal for all BSs,  $U_j^{\text{UL}}$  represents the number of VR users associated with BS  $j$  over uplink,  $\mathcal{U}_j$  is the set of VR users associated with BS  $j$ ,  $P_u$  is the transmit power of each VR user (assumed equal for all users),  $g_{ij}$  is the Rayleigh fading channel gain,  $d_{ij}$  is the distance between VR user  $i$  and BS  $j$  at time  $t$ , and  $\rho^2$  is the noise power.

2) *Downlink VR Video Transmission:* In downlink, antenna arrays are deployed at BSs to perform directional beamforming over the mmWave frequency band. For simplicity, a sectorized antenna model [21] is used to approximate the actual array beam patterns. This simplified antenna model consists of four parameters: the half-power beamwidth  $\phi$ , the boresight direction  $\theta$ , the antenna gain of the mainlobe  $Q$ , and the antenna gain of the sidelobe  $q$ . Let  $\varphi_{ij}$  be the phase from BS  $j$  to VR user  $i$ . The antenna gain of the transmission link from BS  $j$  to user  $i$  is:

$$G_{ij} = \begin{cases} Q, & \text{if } |\varphi_{ij} - \theta_j| \leq \frac{\phi}{2}, \\ q, & \text{if } |\varphi_{ij} - \theta_j| > \frac{\phi}{2}. \end{cases} \quad (2)$$

Since the VR device is located in front of the VR user's head, the mmWave link will be blocked, if the user rotates. Let  $\chi_{it}$  be the orientation of user  $i$  at time  $t$  and  $\vartheta$  be the maximum

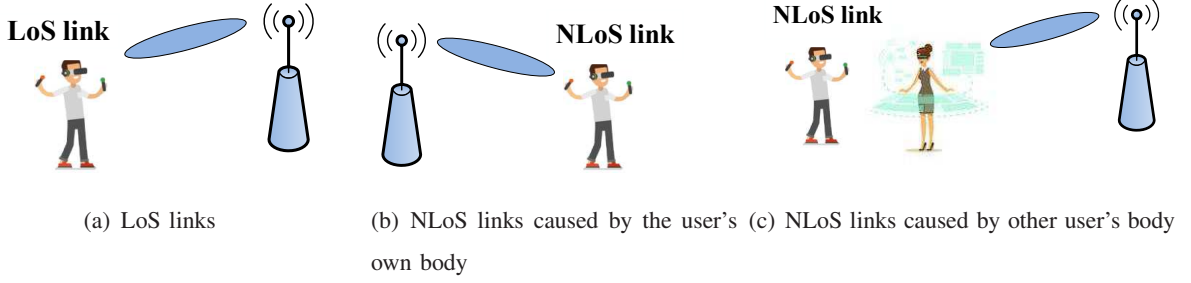


Fig. 2. VR video transmission over LoS/NLoS links

angle using which BS  $j$  can directly transmit VR videos to a user without any human body blockage.  $\phi'_{ij}$  denotes the phase from user  $i$  to BS  $j$ . For user  $i$ , the blockage effect caused by its own body can be given by:

$$b_i(\chi_{it}) = \begin{cases} 1, & \text{if } |\phi'_{ij} - \chi_{it}| \leq \vartheta, \\ 0, & \text{if } |\phi'_{ij} - \chi_{it}| > \vartheta. \end{cases} \quad (3)$$

We assume that each VR user's body constitutes a single blockage area and  $n_{ijt}$  represents the number of VR users located between user  $i$  and BS  $j$  at time  $t$ . If there are no users located between user  $i$  and BS  $j$  that block the mmWave link,  $(b_i(\chi_{it}) + n_{ij} = 0)$ , as shown in Fig. 2(a), the communication link between user  $i$  and BS  $j$  is line-of-sight (LoS). If the mmWave link between user  $i$  and BS  $j$  is blocked by the user  $i$ 's own body (as shown in Fig. 2(b),  $b_i(\chi_{it}) = 1$ ) or blocked by other users located between user  $i$  and BS  $j$  (as shown in Fig. 2(c),  $+n_{ij} > 0$ ), the communication link between user  $i$  and BS  $j$  is said to be non-line-of-sight (NLoS).

Considering path loss and shadowing effects, the path loss for a LoS link and a NLoS link between VR user  $i$  and BS  $j$  in dB will be given by [21]:

$$h_{ij}^{\text{LoS}}(x_{it}, y_{it}) = L_{FS}(d_0) + 10\mu_{\text{LoS}} \log(d_{ij}(x_{it}, y_{it})) + \chi_{\sigma_{\text{LoS}}}, \quad (4)$$

$$h_{ij}^{\text{NLoS}}(x_{it}, y_{it}) = L_{FS}(d_0) + 10\mu_{\text{NLoS}} \log(d_{ij}(x_{it}, y_{it})) + \chi_{\sigma_{\text{NLoS}}}, \quad (5)$$

where  $L_{FS}(d_0)$  represents the free space path loss which can be given by  $20 \log(d_0 f_c 4\pi / \nu)$ . Here,  $d_0$  is the free-space reference distance,  $f_c$  represents the carrier frequency and  $\nu$  is the light speed.  $\mu_{\text{LoS}}$  and  $\mu_{\text{NLoS}}$  represent the path loss exponents for the LoS and NLoS links, respectively.  $\chi_{\sigma_{\text{LoS}}}$  and  $\chi_{\sigma_{\text{NLoS}}}$  are Gaussian random variables in dB with zero mean.  $\sigma_{\text{LoS}}$  and  $\sigma_{\text{NLoS}}$  represent the standard deviations for LoS and NLoS links in dB, respectively. The downlink data rate of



VR video transmission from BS  $j$  to user  $i$  is given by:

$$c_{ij}^{\text{DL}}(x_{it}, y_{it}, b_i(\chi_{it}), n_{ij}) = \begin{cases} F^{\text{DL}} \log_2 \left( 1 + \frac{P_B G_{ij}}{10^{\frac{h_{ij}^{\text{LoS}}}{10}} \rho^2} \right), & \text{if } b_i(\chi_{it}) + n_{ij} = 0, \\ F^{\text{DL}} \log_2 \left( 1 + \frac{P_B G_{ij}}{10^{\frac{h_{ij}^{\text{NLoS}}}{10}} \rho^2} \right), & \text{if } b_i(\chi_{it}) + n_{ij} > 0, \end{cases} \quad (6)$$

where  $F^{\text{DL}}$  is the bandwidth allocated to each user and  $P_B$  is the transmit power of each BS  $j$  which is assumed to be equal for all BSs.

### B. Break in Presence Model

In a VR application, the notion of a BIP represents an event that leads VR users to realize that they are in a fictitious, virtual environment, thus ruining their immersive experience. In other words, a BIP event transitions a user from the immersive virtual world to the real world [22]. For wired VR, BIP can be caused by various factors such as hitting the walls/ceiling, loss of tracking with the device, tripping on wire cords, or talking to another person from the real world [22]. For wireless VR, BIP can be also caused by the delay of VR video and tracking information transmission, the quality of the VR videos received by the VR users, and the inaccurate tracking information received by BSs.

To model such BIPs, we jointly consider the delay of VR video and tracking information transmission and the quality of VR videos. We first define a vector  $\mathbf{l}_{i,t}(c_{ij}^{\text{DL}}(x_{it}, y_{it}, b_i(\chi_{it}), n_{ij})) = [l_{i1,t}, \dots, l_{iN_L,t}]$  that represents a VR video that user  $i$  received at time  $t$  with  $l_{ik,t} \in \{0, 1\}$ .  $l_{ik,t} = 0$  indicates that pixel  $k$  is not successfully received by user  $i$ , and  $l_{ik,t} = 1$ , otherwise. We also define a vector  $\mathbf{m}_{i,t}(G_A) = [m_{i1,t}, \dots, m_{iN_L,t}]^T$  that represents the weight of the importance of each pixel constructing a VR video, where  $m_{ik,t} \in [0, 1]$  and  $G_A$  represents a VR application such as an immersive VR game or a VR video.  $m_{ik,t} = 1$  indicates that pixel  $k$  is one of the most important elements for the generation of  $G_A$ . Here, in each VR application  $G_A$ , a number of pixels can be compressed at the BS and recovered by the user. Hence, the pixels that can be compressed by the BSs not important. However, some of the pixels cannot be compressed by the BS and, hence, they need to transmit to the VR users. Therefore, each pixel will have different importance and  $m_{ik,t} \in [0, 1]$ . Then, the BIP of VR user  $i$  caused by the wireless transmission



will be given by:

$$P_{it}^W(x_{it}, y_{it}, \chi_{it}, \mathbf{a}_{i,t}^{\text{UL}}, \mathbf{a}_{i,t}^{\text{DL}}) = \mathbb{1} \left\{ \frac{A}{a_{ij,t}^{\text{UL}} c_{ij}^{\text{UL}}(x_{it}, y_{it})} + \frac{D(l_{i,t}(a_{ik,t}^{\text{DL}} c_{ik}^{\text{DL}}(x_{it}, y_{it}, b_i(\chi_{it}), n_{ik})))}{a_{ik,t}^{\text{DL}} c_{ik}^{\text{DL}}(x_{it}, y_{it}, b_i(\chi_{it}), n_{ik})} \leq \gamma_D \right\} \vee \mathbb{1} \left\{ l_{i,t}(a_{ik,t}^{\text{DL}} c_{ik}^{\text{DL}}(x_{it}, y_{it}, b_i(\chi_{it}), n_{ik})) m_{i,t}(G_A) \geq \gamma_Q \right\}, \quad (7)$$

where  $\mathbb{1}_{\{x\}} = 1$  as  $x$  is true,  $\mathbb{1}_{\{x\}} = 0$ , otherwise.  $\mathbb{1}_{\{x\}} \vee \mathbb{1}_{\{y\}} = 1$  as  $y$  or  $x$  is true,  $\mathbb{1}_{\{x\}} \vee \mathbb{1}_{\{y\}} = 0$ , otherwise.  $\mathbf{a}_{i,t}^{\text{UL}} = [a_{i1,t}^{\text{UL}}, \dots, a_{iB,t}^{\text{UL}}]$  is a vector that represents user  $i$ 's uplink association with  $a_{ik,t}^{\text{UL}} \in \{0, 1\}$  and  $\sum_{k \in \mathcal{B}} a_{ik,t}^{\text{UL}} = 1$ . Similarly,  $\mathbf{a}_{i,t}^{\text{DL}} = [a_{i1,t}^{\text{DL}}, \dots, a_{iB,t}^{\text{DL}}]$  is a vector that represents user  $i$ 's downlink association with  $a_{ik,t}^{\text{DL}} \in \{0, 1\}$  and  $\sum_{k \in \mathcal{B}} a_{ik,t}^{\text{DL}} = 1$ .  $\gamma_D$  and  $\gamma_Q$  represent the target delay and video quality requirements, respectively. In (7),  $\frac{A}{c_{ij}^{\text{UL}}(x_{it}, y_{it})}$  represents the time used for tracking information transmission from user  $i$  to BS  $j$ .  $\frac{D(l_{i,t}(c_{ik}^{\text{DL}}(x_{it}, y_{it}, b_i(\chi_{it}), n_{ik})))}{c_{ik}^{\text{DL}}(x_{it}, y_{it}, b_i(\chi_{it}), n_{ik})}$  represents the transmission latency for sending the tracking information from BS  $k$  to user  $i$ . For simplicity, hereinafter,  $P_{it}^W$  is referred as  $P_{it}^W(x_{it}, y_{it}, \chi_{it}, \mathbf{a}_{i,t}^{\text{UL}}, \mathbf{a}_{i,t}^{\text{DL}})$ . (7) shows that if the delay of VR video and tracking information transmission exceeds the target delay threshold allowed by VR systems or the quality of VR video cannot meet the video requirement, users will experience a BIP ( $P_{it}^W=1$ ). From (7), we can also see that, the BIP of user  $i$  caused by wireless transmission depends on user  $i$ 's location, orientation, VR applications, and user association. (7) represents the BIP caused by wireless networking factors such as transmission delay and video quality. Next, we show the BIP model that jointly considers wireless transmission, the VR applications, and the users awareness. The BIP of user  $i$  can be given by [23]:

$$P_i(x_{it}, y_{it}, G_A, \chi_{it}, \mathbf{a}_{i,t}^{\text{UL}}, \mathbf{a}_{i,t}^{\text{DL}}) = \frac{1}{T} \sum_{t=1}^T (G_A + P_{it}^W + G_A P_{it}^W + \epsilon_i + \epsilon_{G_A|i} + \epsilon_B), \quad (8)$$

where  $\epsilon_i$  is the user  $i$ 's awareness measured by VR users,  $\epsilon_{G_A|i}$  is joint effect caused by user  $i$ 's awareness and VR application  $G_A$ , and  $\epsilon_B$  is a random effect.  $\epsilon_i$ ,  $\epsilon_{G_A|i}$ , and  $\epsilon_B$  follow the Gaussian distribution [23] with zero mean and variances  $\sigma_i^2$ ,  $\sigma_{G_A|i}^2$ , and  $\sigma_B^2$ , respectively. From (8), we can see that as the VR application for user  $i$  changes, the value of BIP will change. For example, a given user watching VR videos will experience fewer BIPs compared to a user engaged in an immersive first-person shooting game. This is due to the fact that in an immersive game environment, users are fully engaged with the virtual environment, as opposed to some VR applications that require the user to only watch VR videos. In (8), we can also see that the

BIPs depend on the users' awareness. This means that different users will have different actions and perceptions when they interact with the virtual environment and, hence, different VR users may identify different levels of BIP. In (8), the value of  $P_{it}(x_{it}, y_{it}, G_A, \chi_{it}, \mathbf{a}_{i,t}^{\text{UL}}, \mathbf{a}_{i,t}^{\text{DL}})$  quantifies the average number of BIPs that user  $i$  can identify during a period.

### C. Problem Formulation

From (8), we can see that the BIP of each user depends on the user's locations and orientations as well as its associations. Using an effective learning algorithm to predict users' locations and orientations, BSs can proactively determine the users' association to improve the downlink and uplink data rates and minimize BIP for each VR user. The BIP minimization problem can be given as follows:

$$\min_{\hat{x}_{it}, \hat{y}_{it}, \hat{\chi}_{it}, \mathbf{a}_{i,t}^{\text{UL}}, \mathbf{a}_{i,t}^{\text{DL}}} \sum_{i \in \mathcal{U}} P_i(\hat{x}_{it}, \hat{y}_{it}, G_A, \hat{\chi}_{it}, \mathbf{a}_{i,t}^{\text{UL}}, \mathbf{a}_{i,t}^{\text{DL}}) \quad (9)$$

$$\text{s. t.} \quad U_j \leq V, \quad \forall j \in \mathcal{B}, \quad (9a)$$

$$a_{ij,t}^{\text{UL}} \in \{0, 1\}, \quad \forall i \in \mathcal{U}, \forall j \in \mathcal{B}, \quad (9b)$$

$$a_{ij,t}^{\text{DL}} \in \{0, 1\}, \quad \forall i \in \mathcal{U}, \forall j \in \mathcal{B}, \quad (9c)$$

$$\sum_{j \in \mathcal{B}} a_{ij,t}^{\text{UL}} = 1, \quad \forall i \in \mathcal{U}, \quad (9d)$$

$$\sum_{j \in \mathcal{B}} a_{ij,t}^{\text{DL}} = 1, \quad \forall i \in \mathcal{U}, \quad (9e)$$

where  $\hat{x}_{it}$ ,  $\hat{y}_{it}$ , and  $\hat{\chi}_{it}$  are the predicted locations and orientation of user  $i$  at time  $t$ ,  $U_j$  is the number of VR users associated with BS  $j$  over downlink and  $V$  is the maximum number of users that can be associated with each BS. (9b) and (9d) show that each user can associate with only one uplink BS while (9c) and (9e) indicate that each user can associate with only one BS at downlink.

## III. FEDERATED ECHO STATE LEARNING FOR PREDICTIONS OF THE USERS' LOCATION AND ORIENTATION

From (9), we can see that the BIPs of each user will depend on the user association as well as the users' locations and orientations. Meanwhile, the user association depends on the locations and orientations of the VR users. When the user association is not determined, the tracking

information cannot be sent to the BSs. Therefore, the BSs must use historical information related to the users' locations and orientations to determine the user association. As the users' locations and orientations will continuously change as time elapses, BSs must proactively determine the user association to reduce the BIPs of VR users. In consequence, it is necessary to introduce a machine learning algorithm to predict the users' locations and orientations in order to determine the user association and minimize BIPs of VR users. In the model defined in Section II, the user association changes as the users' location or orientation vary with time. Consequently, each BS that connects to a given VR user can only collect partial information about this user's mobility patterns and orientation. However, a BS cannot rely on partial information to predict each user's location and orientation. Moreover, since a given VR user will change its association, the data pertaining to this VR user's movement will be located at multiple BSs. Hence, traditional centralized learning algorithms that are implemented by a given BS cannot predict the entire VR user's mobility patterns and orientations without knowing the user's data collected by other BSs. To overcome the challenges mentioned previously, we introduce an ESN-based distributed federated learning framework that can predict the location and orientation of each VR user as the training data related to each user's locations and orientations is located at multiple BSs.

*Federated learning* is a decentralized learning algorithm [24] that can operate by using training datasets that are distributed across multiple devices (e.g., BSs), instead of being centralized at one location or device [25]. For our system, one key advantage of federated learning is that it can allow multiple BSs to locally train their ESNs using their collected data and cooperatively build a learning model by sharing their locally trained models. Compared to existing federated learning algorithms [25] that use matrices to record the users' behavior and cannot analyze the correlation of the users' behavior data, we propose an ESN-based federated learning algorithm that can use an ESN to efficiently analyze the data related to the users' mobility and orientation since an ESN that is a recurrent neural network is good at analyzing time-related data. Moreover, ESNs only need to train an output weight matrix, hence, they reduce the training complexity of the federated learning algorithms. Next, we first introduce the components of the federated ESN learning model. Then, we explain the entire procedure of using our federated ESN learning algorithm to predict the users' mobility patterns and orientation.

### A. Components of Federated ESN Learning Algorithm

A federated ESN learning algorithm consists of four components: a) agents, b) input, c) output, and d) local ESN model, which are specified as follows:

- *Agent*: In our system, we need to define an individual federated ESN learning algorithm to predict the mobility and orientation of each VR user. Meanwhile, each user's individual federated ESN learning algorithm must be implemented by all BSs that have been associated with this user. Hence, each BS  $j$  must implement at most  $U$  learning algorithms.
- *Input*: The input of the federated ESN learning algorithm that is implemented by BS  $j$  for the predictions of each VR user  $i$  is defined by a vector  $\mathbf{x}_{ij} = [\mathbf{x}_{ij,1}, \dots, \mathbf{x}_{ij,T}]^T$  that represents the information related to user  $i$ 's mobility and orientation where  $\mathbf{x}_{ij,t} = [\xi_{ij1,t}, \dots, \xi_{ijN_x,t}]$  represents user  $i$ 's information related to mobility and orientation at time  $t$ . This information includes user  $i$ 's locations, orientations, VR applications, and the time that user  $i$  associates with BS  $j$ .  $N_x$  is the number of properties that constitute a vector  $\mathbf{x}_{ij,t}$ . The input of the proposed algorithm will be combined with the ESN model to predict users' orientation and mobility patterns. BSs will use these predictions to determine user associations.
- *Output*: For each user  $i$ , the output of the federated ESN learning algorithm at BS  $j$  is a vector  $\mathbf{y}_{ij,t} = [\hat{\mathbf{y}}_{ijt+1}, \dots, \hat{\mathbf{y}}_{ijt+Y}]$  of user  $i$ 's locations and orientations where  $\hat{\mathbf{y}}_{ijt+k} = [\hat{x}_{it+k}, \hat{y}_{it+k}, \hat{\chi}_{it+k}]$  with  $\hat{x}_{it+k}$  and  $\hat{y}_{it+k}$  being the predicted location coordinates of user  $i$  at time  $t+k$  and  $\hat{\chi}_{it+k}$  being the estimated orientation of user  $i$  at  $t+k$ .  $Y$  is the number of future time slots that a federated ESN learning algorithm can predict. The predictions of the locations and orientations can be used to determine the user's association.
- *Local ESN model*: For each BS  $j$ , a local ESN model is used to build the relationship between the input of all BSs and the predictions of the users' mobility and orientation, as shown in Fig. 4. The local ESN model consists of the input weight matrix  $\mathbf{W}_j^{\text{in}} \in \mathbb{R}^{N_W \times T}$ , recurrent matrix  $\mathbf{W}_j \in \mathbb{R}^{N_W \times N_W}$ , and the output weight matrix  $\mathbf{W}_j^{\text{out}} \in \mathbb{R}^{Y \times (N_W + T)}$ . The values of  $\mathbf{W}_j^{\text{in}}$  and  $\mathbf{W}_j$  are generated randomly. However, the output weight matrix  $\mathbf{W}_j^{\text{out}}$  need to be trained according to the inputs of all BSs.

We introduce three ESN models: *single ESN model*, *series ESN model*, and *parallel ESN model*. In the single ESN model, an ESN is directly connected to the input and output. Moreover, as shown in Fig. 3, series and parallel ESN models connect single ESN models

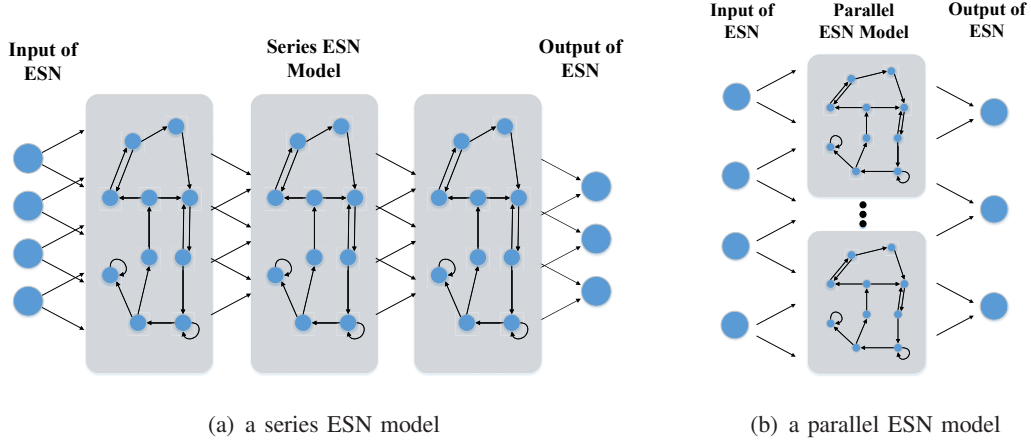


Fig. 3. Architectures of deep ESN models.

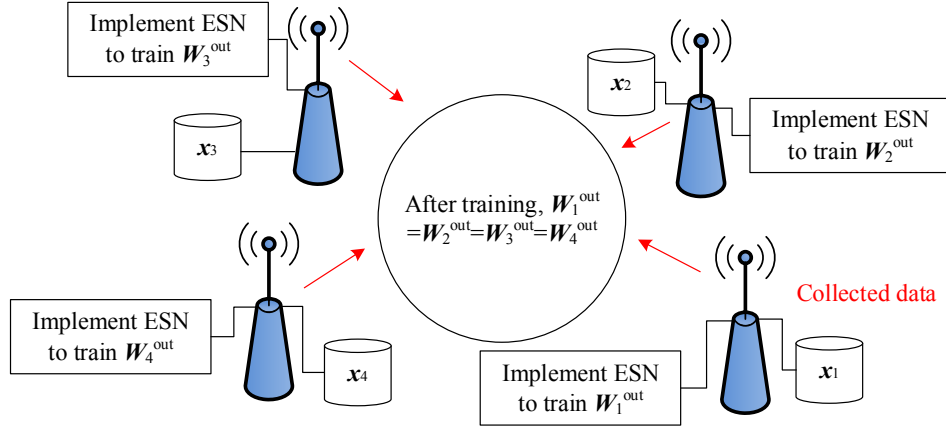


Fig. 4. The implementation of the ESN based federated learning.

in series and parallel, respectively.

### B. ESN Based Federated Learning Algorithm for Users' Location and Orientation Predictions

Next, we explain the entire procedure of training ESN based federated learning algorithm. Our purpose of training ESN is to find an optimal output weight matrix in order to accurately predict the users' mobility patterns and orientations, as shown in Fig. 4.

To introduce the training process, we first explain the state of the neurons in ESN. The neuron states of the proposed algorithm implemented by BS  $j$  for the predictions of user  $i$  are:

$$\mu_{j,t} = W_j \mu_{j,t-1} + W_j^{\text{in}} x_{ij,t}. \quad (10)$$

Based on the states of neurons and the inputs, the ESN can estimate the output, which will is:

$$\hat{y}_{ij,t} = W_{j,t}^{\text{out}} \begin{bmatrix} x_{ij,t} \\ \mu_{j,t} \end{bmatrix}. \quad (11)$$

From (11), we can see that to enable an ESN to predict the users' mobility patterns and orientations, we only need to adjust the value of the output weight matrix. However, each BS can collect only partial data for each user and, hence, we need to use a distributed learning algorithm to train the ESNs. To introduce the distributed learning algorithm, we first define two matrices which are given by:

$$\mathbf{H}_j = \begin{bmatrix} \mathbf{x}_{ij,1} & \boldsymbol{\mu}_{j,1} \\ \vdots & \vdots \\ \mathbf{x}_{ij,T} & \boldsymbol{\mu}_{j,T} \end{bmatrix} \text{ and } \mathbf{E}_j = [\mathbf{e}_{ij,1}, \dots, \mathbf{e}_{ij,T}], \quad (12)$$

where  $\mathbf{e}_{ij,t}$  is the desired locations and orientations of each VR user, given the ESN input  $\mathbf{x}_{ij,t}$ . Then, the training purpose can be given as follows:

$$\min_{\mathbf{W}^{\text{out}}} \frac{1}{2} \left( \sum_{j=1}^B \|\mathbf{W}^{\text{out}} \mathbf{H}_j^T - \mathbf{E}_j\|^2 \right) + \frac{\lambda}{2} \|\mathbf{W}^{\text{out}}\|. \quad (13)$$

(13) is used to find the optimal output weight matrix  $\mathbf{W}^{\text{out}}$  according to which the BSs can predict the entire users' locations and orientations without the knowledge of the users' data collected by other BSs. From (13), we can see that, each BS  $j$  needs to adjust its output weight matrix  $\mathbf{W}_j^{\text{out}}$  and find the optimal output weight matrix  $\mathbf{W}^{\text{out}}$ . The update of  $\mathbf{W}_j^{\text{out}}$  is given by:

$$\mathbf{W}_{j,t+1}^{\text{out}} = \varsigma^{-1} [\mathbf{I} - \mathbf{H}_j^T (\varsigma \mathbf{I} + \mathbf{H}_j \mathbf{H}_j^T) \mathbf{H}_j^T] (\mathbf{H}_j^T \mathbf{E}_j - \mathbf{n}_{j,t} + \varsigma \mathbf{W}_t^{\text{out}}), \quad (14)$$

where  $\varsigma$  is the learning rate and  $\mathbf{W}_t^{\text{out}}$  is the optimal output weight matrix that the ESN model of each BS needs to find. From (14), we can see that  $\mathbf{W}_{j,t+1}^{\text{out}}$  is the output weight matrix that is generated at BS  $j$ .  $\mathbf{W}_{j,t+1}^{\text{out}}$  can only be used to predict partial mobility patterns and orientations given the users' data collected by BS  $j$ .  $\mathbf{W}_{j,t+1}^{\text{out}}$  is different from the output weight matrices of other BSs. The optimal output weight matrix is given by:

$$\mathbf{W}_{t+1}^{\text{out}} = \frac{B\varsigma \hat{\mathbf{W}}_{t+1}^{\text{out}} + B\hat{\mathbf{n}}_t}{\lambda + \varsigma B}, \quad (15)$$

where  $\hat{\mathbf{W}}_{t+1}^{\text{out}}$  and  $\hat{\mathbf{n}}_{t+1}^{\text{out}}$  can be calculated as follows:

$$\hat{\mathbf{W}}_{t+1}^{\text{out}} = \frac{1}{B} \sum_{j=1}^B \mathbf{W}_{j,t+1}^{\text{out}}, \quad \hat{\mathbf{n}}_t = \frac{1}{B} \sum_{j=1}^B \mathbf{n}_{j,t}. \quad (16)$$

In (14),  $\mathbf{n}_{j,t}$  is the deviation between the output weight matrix  $\mathbf{W}_{j,t+1}^{\text{out}}$  of each BS  $j$  and the optimal output weight matrix  $\mathbf{W}_{t+1}^{\text{out}}$  that the ESN model of each BS needs to converge, which

---

**Algorithm 1** Federated ESN learning algorithm for mobility and orientation predictions
 

---

**Input:** Training data set (local),  $\mathbf{x}_{ij}$ .

**Initialization:** Each BS  $j$  generates the ESN model for each user including  $\mathbf{W}_j^{\text{in}}$  (local),  $\mathbf{W}_j$  (global), and  $\mathbf{W}_j^{\text{out}}$  (local).

- 1: Obtain the matrices  $\mathbf{H}_j$  and  $\mathbf{E}_j$  based on (10).
  - 2: **for** time  $t$  **do**
  - 3:   Compute  $\mathbf{W}_{j,t+1}^{\text{out}}$  using (14).
  - 4:   Calculate  $\hat{\mathbf{W}}_{t+1}^{\text{out}}$  and  $\hat{\mathbf{n}}_t^{\text{out}}$  based on (16).
  - 5:   Calculate  $\mathbf{W}_{t+1}^{\text{out}}$  based on (15).
  - 6:   Compute  $\mathbf{n}_{j,t+1}$  based on (17).
  - 7:   Compute  $\|\mathbf{r}_{j,t+1}\|$  and  $\|\mathbf{s}_{j,t}\|$ .
  - 8:   If  $\|\mathbf{r}_{j,t+1}\| \leq \gamma_A$  or  $\|\mathbf{s}_{j,t}\| \leq \gamma_A$ , the algorithm converges.
  - 9: **end for**
- 

is given by:

$$\mathbf{n}_{j,t+1} = \mathbf{n}_{j,t} + \gamma (\mathbf{W}_{j,t+1}^{\text{out}} - \mathbf{W}_{t+1}^{\text{out}}). \quad (17)$$

$\mathbf{W}_{t+1}^{\text{out}}$  is the global optimal output weight matrix that can be used to predict the entire mobility patterns and orientations of a given user. This means that using  $\mathbf{W}_{t+1}^{\text{out}}$ , each BS can predict the entire user's mobility patterns and orientations as the BS only collects partial data related to the user's mobility and orientations. As time elapses,  $\mathbf{W}_{j,t+1}^{\text{out}}$  will finally converge to  $\mathbf{W}_{t+1}^{\text{out}}$ . In consequence, all of BSs can predict the entire mobility patterns and orientations of each user. To measure the convergence, we define two vectors which can be given by  $\mathbf{r}_{j,t} = \mathbf{W}_{j,t}^{\text{out}} - \mathbf{W}_t^{\text{out}}$  and  $\mathbf{s}_{j,t} = \mathbf{W}_t^{\text{out}} - \mathbf{W}_{t-1}^{\text{out}}$ . As  $\|\mathbf{r}_{j,t+1}\| \leq \gamma_A$  or  $\|\mathbf{s}_{j,t}\| \leq \gamma_A$ , the proposed algorithm converges.  $\gamma_A$  is determined by the BSs. As  $\gamma_A$  increases, the accuracy of the predictions and the number of iterations decrease. Therefore, BSs need to jointly account for the time used for training ESN and the prediction accuracy to determine the value of  $\gamma_A$ . As the learning algorithm converges, each BS can use its own ESN to predict the entire mobility and orientation of each VR user. According to these predictions, BSs can determine the user association to minimize the BIPs of VR users. Algorithm 1 summarizes the entire process of using ESN based federated learning algorithm for the predictions of the users' mobility patterns and orientations. From Algorithm 1, we can see that  $\mathbf{W}_j^{\text{in}}$  and  $\mathbf{W}_j^{\text{out}}$  are local parameters which means that each BS  $j$  will generate its own  $\mathbf{W}_j^{\text{in}}$  and  $\mathbf{W}_j^{\text{out}}$ . However,  $\mathbf{W}_j$  is a global parameter which means that all of the BSs will have the same  $\mathbf{W}_j$ .



#### IV. MEMORY CAPACITY ANALYSIS FOR ECHO STATE NETWORK BASED FEDERATED LEARNING ALGORITHM

To improve the prediction accuracy of the proposed ESN based federated learning algorithm, in this section, we analyze the memory capacity of the proposed ESN model. The memory capacity quantifies the ability of each ESN to record the historical locations and orientations of each VR user. As the memory capacity of the ESNs increases, the ESNs can record more historical data related to users' mobility and use this information to achieve better prediction for the users' location and orientation. Next, we derive closed-form expressions of the memory capacity of the three ESN models that we described in Section III, namely, the single ESN model, the parallel ESN model, and the series ESN model.

We assume that the input of each ESN model at time  $t$  is  $m_t$  and the output of each ESN model is  $z_t$ . Then, the memory capacity of each ESN model is given by [26]:

$$M = \sum_{k=1}^{\infty} \frac{\text{Cov}^2(m_{t-k}, z_t)}{\text{Var}(m_t)\text{Var}(z_t)}, \quad (18)$$

where Cov and Var represent the covariance and variance operators, respectively. The recurrent matrix  $\mathbf{W}$  in each ESN model can be given by

$$\mathbf{W}_l = \begin{bmatrix} 0 & 0 & \cdots & w \\ w & 0 & 0 & 0 \\ 0 & \ddots & 0 & 0 \\ 0 & 0 & w & 0 \end{bmatrix}, \quad (19)$$

and the input weight matrix is given by  $\mathbf{W}^{\text{in}} = [w_1^{\text{in}}, \dots, w_{N_W}^{\text{in}}]^T$ . We also define a matrix that will be used to derive the memory capacity of the ESNs, which can be given by:

$$\mathbf{V} = \begin{bmatrix} w_1^{\text{in}} & w_{N_W}^{\text{in}} & \cdots & w_2^{\text{in}} \\ w_2^{\text{in}} & w_1^{\text{in}} & \cdots & w_3^{\text{in}} \\ \vdots & \vdots & \cdots & \vdots \\ w_{N_W}^{\text{in}} & w_{N_W-1}^{\text{in}} & \cdots & w_1^{\text{in}} \end{bmatrix}. \quad (20)$$

Based on the above definitions, we can invoke our result from [26, Theorem 2] to derive the memory capacity of single ESN model, which can be given as follows.

**Corollary 1** (Single ESN model). Given the recurrent matrix  $\mathbf{W}$  and the input matrix  $\mathbf{W}^{\text{in}}$  that guarantees the matrix  $\mathbf{V}$  regular, the memory capacity of the single ESN model is:

$$M = N_W - 1 + w^{2N_W}. \quad (21)$$

*Proof.* We can directly invoke the result of [26, Theorem 2], which shows that the memory capacity of the single ESN model can be given by  $M = \sum_{k=0}^{N_W-1} \left( \sum_{j=0}^{\infty} \mathbb{E}[w^{2N_W j + 2k}] \right)^{-1} \sum_{j=0}^{\infty} \mathbb{E}[w^{N_W j + k}]^2 - \left( \sum_{j=0}^{\infty} \mathbb{E}[w^{2N_W j}] \right)^{-1}$ . Since  $w$  is a constant,  $\mathbb{E}[w^k] = w^k$  and, hence,  $M = N_W - 1 + w^{2N_W}$ . This completes the proof.  $\square$

From Corollary 1, we can see that the memory capacity of the single ESN model depends on the number of neurons and values of the recurrent matrix. Corollary 1 also shows that the memory capacity of the single ESN model will not exceed  $N_W$ . That means the single ESN model based federated learning algorithm can only record  $N_W$  mobility patterns or orientations.

Next, we derive the memory capacity of the parallel ESN model, which can be given by the following theorem.

**Theorem 1** (Parallel ESN). Given a parallel ESN model during which  $L$  ESN models are parallel connected with each other, each ESN model's input weight matrix  $\mathbf{W}^{\text{in}}$  that guarantees the matrix  $\mathbf{V}$  regular and recurrent matrix  $\mathbf{W}$ , then the memory capacity of each parallel ESN can be given by:

$$M = N_W - 1 + w^{2N_W}. \quad (22)$$

*Proof.* See Appendix A.  $\square$

From Theorem 1, we can see that the memory capacity of a parallel ESN model is similar to the memory capacity of a single ESN. This means that adding multiple ESN models will not increase the memory capacity. This is due to the fact that, in a parallel ESN model, there is no connection among the ESNs, as shown in Fig. 3(b). Therefore, the input of the parallel ESN model will separately connect to each single ESN and, hence, the parallel ESN models do not need to use more neurons to record the input data compared to the single ESN model. Theorem 1 also shows that the memory capacity of a parallel ESN depends on the number of neurons in each ESN model and the values of the recurrent weight matrix of each ESN model. Accordingly, we can increase the value of output weight matrix and the number of neurons in

each ESN model to increase the memory capacity of the parallel ESN models. As the memory capacity of the parallel ESN models increases, BSs can record more users' data to predict the users' mobility and orientations accurately. Next, we derive the memory capacity of the series ESN model.

**Theorem 2** (Series ESN model). Given a series ESN model during which  $L$  ESN models are series connected with each other, a recurrent matrix  $\mathbf{W}$  of each ESN model, and each ESN model's input weight matrix  $\mathbf{W}^{\text{in}}$  that guarantees the matrix  $\mathbf{V}$  regular, the memory capacity of each series ESN model is

$$M = (1 - w^{2N_W})^{L-1} (N_W - 1 + w^{2N_W}). \quad (23)$$

*Proof.* See Appendix B. □

From Theorem 2, we can see that the memory capacity of each series ESN model is smaller than the memory capacity of a single ESN or a series ESN. Theorem 2 also shows that the memory capacity of each series ESN model decreases as the number of ESN models  $L$  increases. Thus, it would be better to use a single ESN model or a parallel ESN model to predict the users' mobility and orientations.

Theorems 1 and 2 derive the memory capacities of the parallel ESN model and the series ESN model with single input. Next, we formulate the memory capacity of a single ESN model given multiple inputs, which is given by the following theorem.

**Theorem 3** (Multi-input single ESN). Consider a single ESN with a recurrent matrix  $\mathbf{W}$ , input vector  $\mathbf{m}_t = [m_{1t}, \dots, m_{Kt}]$ , the input weight matrix  $\mathbf{W}^{\text{in}}$  that guarantees the matrix  $\mathbf{V}$  regular, the memory capacity of each single ESN is

$$M = \left( \frac{\sum_{l=1}^K \sigma_l^2}{\sum_{k=1}^K \sum_{n=1}^K \rho_{kn} \sigma_k \sigma_n} \right)^2 (N_W - 1 + w^{2N_W}), \quad (24)$$

where  $\rho_{kn}$  represents the correlation coefficient between input  $m_{kt}$  and  $m_{nt}$ .

*Proof.* See Appendix C. □

From Theorem 3, we can observe that the correlation among input elements in vector  $\mathbf{m}_t$  will affect the memory capacity of each ESN model. In particular, as the correlation of the input data increases, the memory capacity of the ESN model increases. This is because the ESN can use

more input data to predict the users' mobility and orientations, hence improving the predictions accuracy. Therefore, it would be better to jointly predict the users' mobility and orientation.

Theorems 1-3 allow each BS to determine its ESN model, the number of neurons  $N_W$  in each ESN model, and the values of the recurrent matrix  $\mathbf{W}$  as the size of the data collected by each BS changes. Since a parallel ESN model has a larger memory capacity compared with the series ESN model and is more stable than the single ESN model, we use the parallel ESN model in our proposed algorithm.

## V. USER ASSOCIATION FOR VR USERS

Based on the analysis presented in Sections III and IV, each BS can predict the users' mobility patterns and orientations. Next, we explain how to use these predictions to find the user association for each VR user. Given the predictions of the mobility and orientations, the BIP minimization problem in (9) can be rewritten as follows:

$$\min_{\mathbf{a}_{i,t}^{\text{UL}}, \mathbf{a}_{i,t}^{\text{DL}}} \sum_{i \in \mathcal{U}} P_i(\hat{x}_{it}, \hat{y}_{it}, G_A, \hat{\chi}_{it}, \mathbf{a}_{i,t}^{\text{UL}}, \mathbf{a}_{i,t}^{\text{DL}}). \quad (25)$$

The user association for each VR user  $i$  at time  $t$  can be determined by the following theorem.

**Theorem 4.** Given the predicted location and orientation of user  $i$  at time  $t$ , the uplink and downlink cell association for a VR user  $i$  is:

$$a_{i*,t}^{\text{UL}} = \mathbb{1} \left\{ a_{ij,t}^{\text{UL}} = \arg \min_{a_{ij,t}^{\text{UL}}} \frac{A}{a_{ij,t}^{\text{UL}} c_{ij}^{\text{UL}}(\hat{x}_{it}, \hat{y}_{it})} \right\}, \quad (26)$$

$$a_{ik,t}^{\text{DL}} = \mathbb{1} \left\{ \frac{D(\mathbf{l}_{i,t}(a_{ik,t}^{\text{DL}} c_{ik}^{\text{DL}}(\hat{x}_{it}, \hat{y}_{it}, b_i(\hat{\chi}_{it}), n_{ik})))}{a_{ik,t}^{\text{DL}} c_{ik}^{\text{DL}}(\hat{x}_{it}, \hat{y}_{it}, b_i(\hat{\chi}_{it}), n_{ik})} \leq \gamma_D - \frac{A}{a_{i*,t}^{\text{UL}} c_{i*}^{\text{UL}}(\hat{x}_{it}, \hat{y}_{it})} \right\} \wedge \mathbb{1} \left\{ \mathbf{l}_{i,t}(a_{ik,t}^{\text{DL}} c_{ik}^{\text{DL}}(\hat{x}_{it}, \hat{y}_{it}, b_i(\hat{\chi}_{it}), n_{ik})) \mathbf{m}_{i,t}(G_A) \geq \gamma_Q \right\}, \quad (27)$$

where  $a_{i*,t}^{\text{UL}}$  and  $a_{ik,t}^{\text{DL}}$  are the uplink and downlink user association obtained in (26) and (27), respectively.  $c_{i*}^{\text{UL}}(x_{it}, y_{it})$  is the uplink data rate of user  $i$ .

*Proof.* See Appendix D. □

From Theorem 4, we can see that the user association of each user  $i$  depends on user  $i$ 's location and orientation. Theorem 4 also shows that, for uplink, each user  $i$  will find at most one BS to connect. The uplink association is determined based on the minimum distance. Theorem 4 also shows that, for each user  $i$ , the uplink user association will affect the downlink user

TABLE II  
SYSTEM PARAMETERS

Parameter	Value	Parameter	Value	Parameter	Value
$P_B$	30 dBm	$d_0$	5 m	$Y$	10
$P_U$	10 dBm	$f_c$	28 GHz	$T$	5
$\sigma$	-94 dBm	$c$	$3 \times 10^8$ m/s	$\gamma$	0.5
$F^{\text{UL}}$	10 Mbit	$\mu_{\text{LoS}}, \mu_{\text{NLoS}}$	2, 2.4	$\lambda$	0.005
$F^{\text{DL}}$	10 Mbit	$\chi_{\sigma_{\text{LoS}}}, \chi_{\sigma_{\text{NLoS}}}$	5.3, 5.27	$w$	0.98
$N_W$	30	$G_A$	11	$L$	3
$\beta$	2	$\gamma_D$	10 ms	$V$	10
$M$	15 dB	$\gamma_Q$	0.8	$\vartheta$	2
$m$	0.7 dB	$\sigma_i^2$	0.193	$\sigma_{G_A i}^2$	0.151
$\phi$	$30^\circ$	$A$	50 kbits	$\sigma_B^2$	0.05

association. This is due to the fact that the VR system has determined the total transmission delay of each user. As a result, when the uplink user association is determined, the uplink transmission delay and the requirement of the downlink transmission delay will be determined. Based on Theorem 4, we use a reinforcement learning algorithm given in [27] to find a sub-optimal solution. The reinforcement learning algorithms can learn the VR users state and exploit different actions to adapt the user association according to the the predictions of the users' mobility and orientation. After the learning step, each BS will find a sub-optimal user association to service the VR users.

## VI. SIMULATION RESULTS

For our simulations, we consider a circular area with radius  $r = 500$  m,  $U = 20$  wireless VR users, and  $B = 5$  BSs distributed uniformly. Real data traces for pedestrian mobility are collected from 50 students at the Beijing University of Posts and Telecommunications. The daily mobility pattern of each student is collected every hour during 9:00 am - 9:00 pm. The orientation data is collected from a first-person shooter game at the Youtube Website. In particular, we record the users' orientations from 25 videos of the first-person shooter VR game. In simulations, a parallel ESN model is used for the proposed algorithm due to its stability and large memory capacity. The detailed system parameters are listed in Table II. For comparison purposes, we consider the deep learning algorithm in [13] and the ESN algorithm in [14], as two baseline schemes. All statistical results are averaged over a large number of independent runs.

Figs. 5 and 6 show the predictions of the VR users' locations and orientations as time elapses.

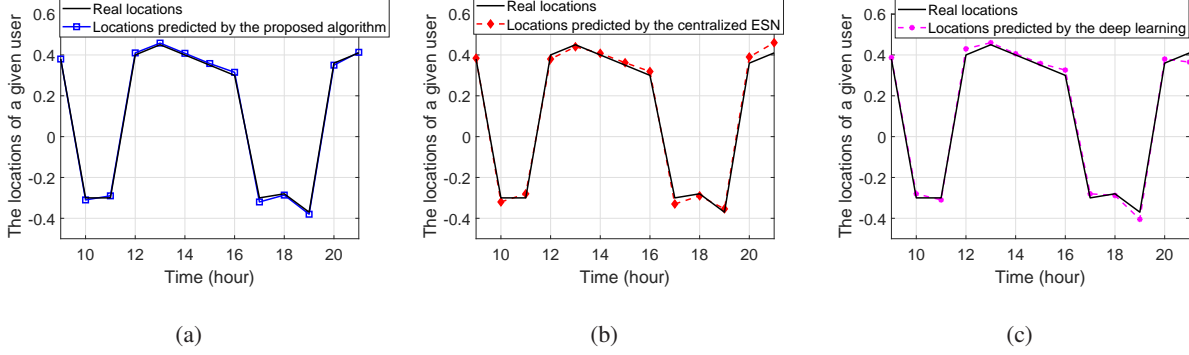


Fig. 5. Predictions of the VR users' orientations and mobility patterns as time elapses.

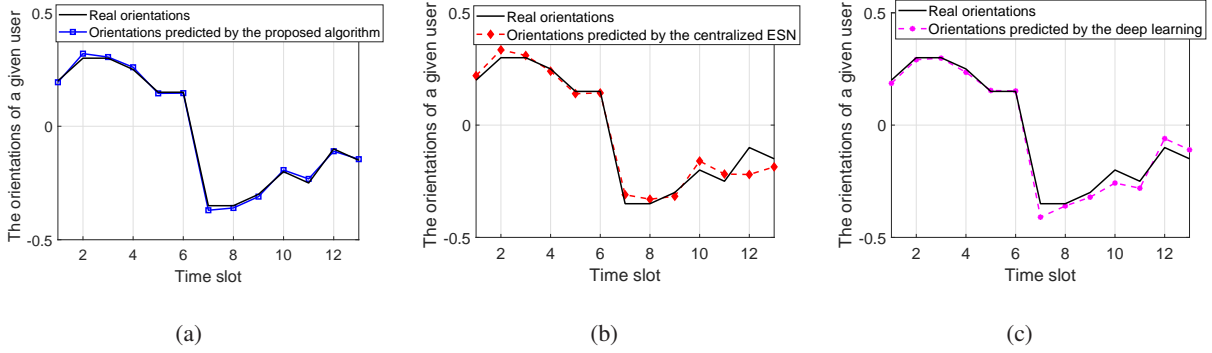


Fig. 6. Predictions of the VR users' orientations and mobility patterns as time elapses.

To simplify the model training, the collected data related to locations and orientations are mapped to  $[-0.5, 0.5]$ . From Figs. 5 and 6, we observe that the proposed algorithm can predict the users' locations and orientations more accurately than the centralized ESN and deep learning algorithms. Figs. 6(b) and 6(c) also show that the prediction error mainly occur at time slot 8 to 12. This is due to the fact that the proposed algorithm can build a learning model that predicts the entire mobility and orientation of each user. In particular, the output weight matrices of all ESN algorithms implemented by each BS will converge to a common matrix. Hence, BSs can predict the entire mobility and orientations of each VR user.

Fig. 7 shows how the total BIP of all VR users changes as the number of BSs varies. From Fig. 7, we can see that, as the number of BSs increases, the total BIP of all VR users decreases. That is because as the number of BSs increases, the VR users have more connection options. Hence, the blockage caused by human bodies will be less severe, thereby improving the data rates of VR users. Fig. 7(a) also shows that the proposed algorithm can achieve up to 16% and 26% reduction in the number of BIPs, respectively, compared to centralized ESN algorithm and deep learning algorithm for a network with 9 BSs. These gains stem from the fact that the centralized ESN and deep learning algorithms can partially predict the mobility and orientation

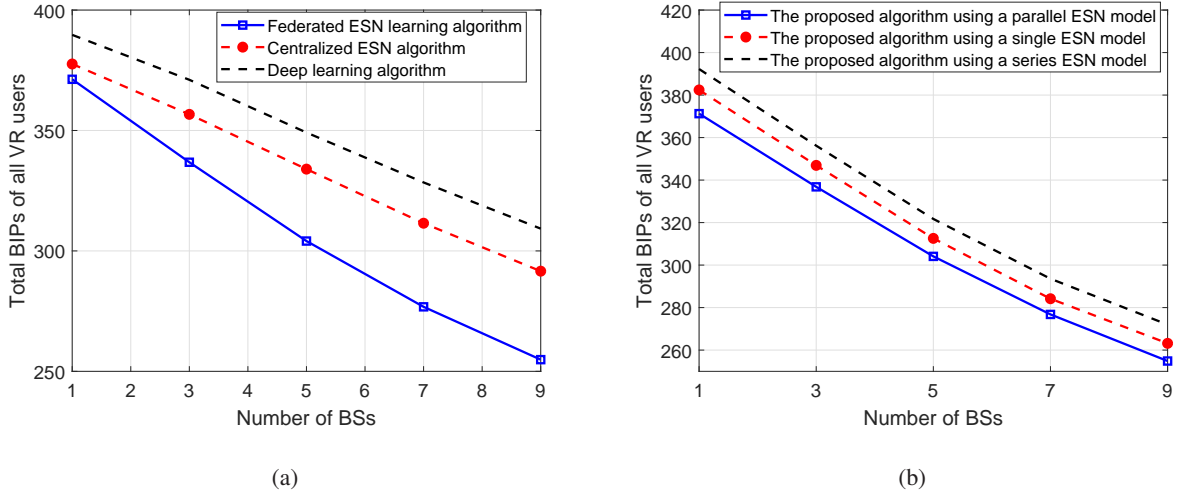


Fig. 7. Total BIPs experienced by VR users as the number of BSs varies.

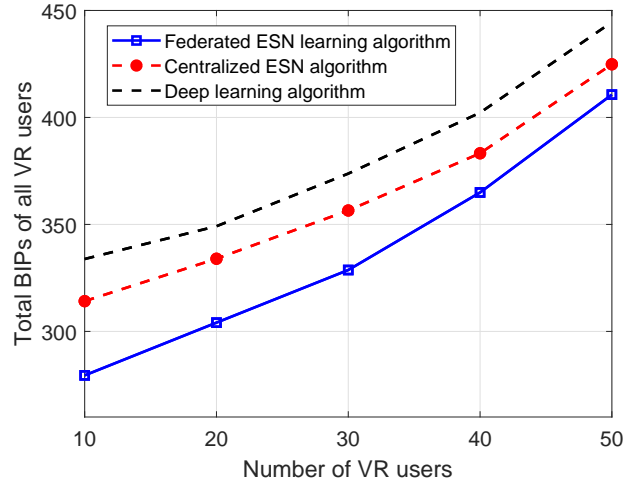


Fig. 8. Total BIP of all VR users as the number of VR users varies.

of each VR user as they rely only on the local data collected by a BS. In contrast, the proposed algorithm facilitates cooperation among BSs to build a learning model that can predict the entire users' mobility and orientations. Fig. 7(b) shows that the proposed algorithm using a parallel ESN model can achieve up to 8% and 14% gains in terms of the total BIPs of all users compared to the proposed algorithm with a single ESN model and with a series model. Clearly, compared to a single ESN, using a parallel ESN model can increase the stability of the proposed algorithm. Meanwhile, the memory capacity of a parallel model is larger than a series ESN model thus improving the prediction accuracy and reducing BIPs for users.

In Fig. 8, we show how the total BIPs of all VR users changes with the number of VR users. This figure shows that, with more VR users, the total BIP of all VR users increases rapidly due



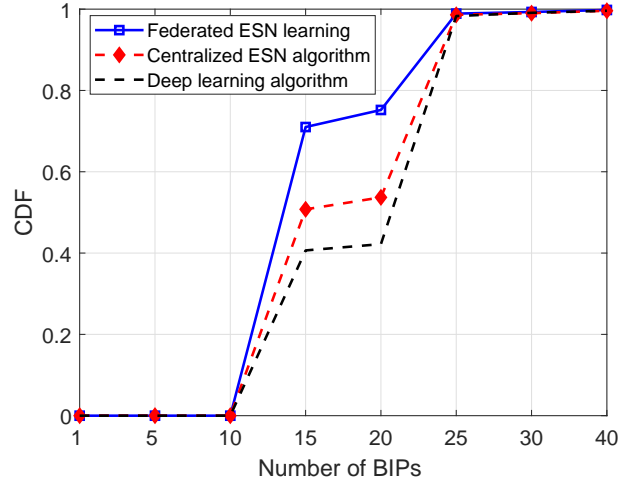


Fig. 9. CDFs of the BIP resulting from the different algorithms.

to an increase in the uplink delay, as the sub-6 GHz bandwidth is shared by more users. Fig. 8 also shows that the gap between the proposed algorithm and the centralized ESN algorithm decreases as more VR users are present in the network.. Clearly, with more VR users, it becomes more probable that a user located between a given VR user and its associated BS blocks the mmWave link. Thus, as the number of users increases, more VR users will receive their VR videos over NLoS links and, the total BIPs significantly increases.

In Fig. 9, we show the CDF for the VR users' BIP for all three algorithms. Fig. 9 shows that the BIP of almost 98% of users resulting from the considered algorithms will be larger than 10. This is due to the fact that the BIP will also be caused by other factors such as VR applications and user's awareness. In Fig. 9, we can also see that the proposed algorithm improves the CDF of up to 38% and 71% gains at a BIP of 15 compared to the centralized ESN and deep learning algorithms, respectively. These gains stem from the fact the ESNs are effective at analyzing the time related mobility and orientation data and, hence, they can accurately predict the users' mobility and orientation.

Fig. 10 shows how the normalized root mean square error (NRMSE) of the predictions changes as the number of neurons in each ESN model varies. In this figure, the NRMSE of the predictions is given by  $\|\hat{\mathbf{y}}_{ij,t} - \mathbf{e}_{ij,t}\|$ . From Fig. 10, we can see that, with more neurons, the NRMSE of the predictions resulting from all of the considered ESN models decreases. This is because, as the number of neurons increases, each ESN model can record more historical data related to the

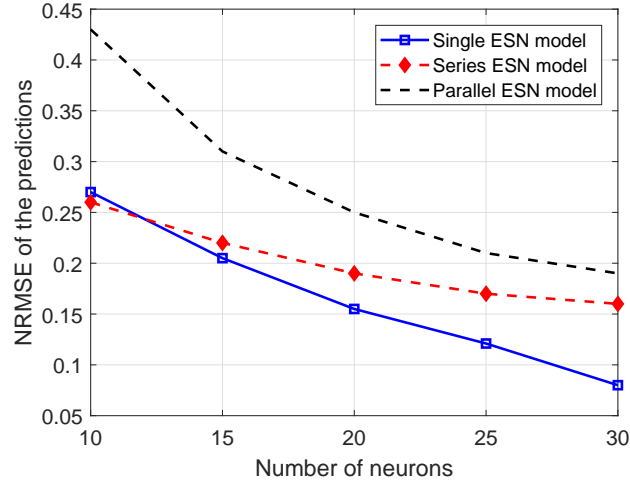


Fig. 10. Normalized root mean square error of the predictions as the number of neurons varies.

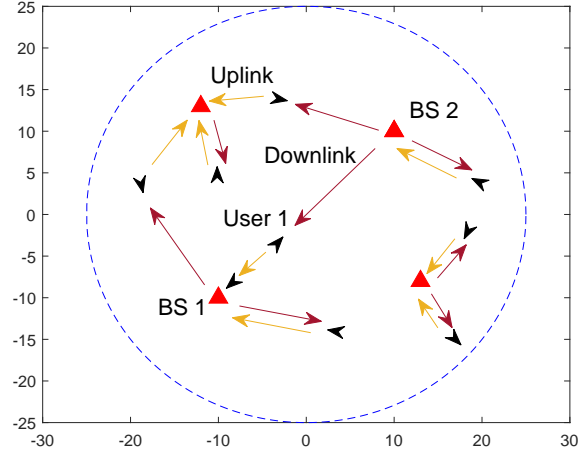


Fig. 11. An example scenario for user association.

users' mobility and orientations. Fig. 10 also shows that the parallel model can achieve up to 37.5% and 90% gains in terms of NRMSE compared to the series model for the ESN models have 30 neurons. This is due to the fact that the prediction errors of a parallel ESN model is averaged over multiple outputs, thus, improving the prediction accuracy.

Fig 11 shows an example of user association scenario based on the proposed framework. In this figure, black arrow denotes the VR users and the direction of the arrows shows the orientations of VR users. From Fig. 11, we can see that user 1 is located closer to BS 1 than BS 2. However, user 1 associates with BS 2 in the downlink and connects with BS 1 in the uplink. This is due to the presence of a blocking user between user 1 and BS 1, as well as the fact that

user 1's orientation is towards BS 2. Thus, the downlink mmWave transmission link between user 1 and BS 1 is NLoS. Since there are no users located between user 1 and BS 2 and the orientation of user 1 is aligned toward BS 2, the downlink mmWave transmission link between user 1 and BS 2 is LoS. Hence, user 1 associates with BS 2 in the downlink. For uplink, since the sub-6 GHz band will not be affected by the body blockage, user 1 will associate with BS 1.

## VII. CONCLUSION

In this paper, we have developed a novel framework for minimizing BIPs within VR applications that operate over wireless cellular networks. To this end, we have developed a BIP model that jointly considers the VR applications, transmission delay, VR video quality, and the user's awareness. We have then formulated an optimization problem that seeks to minimize the BIP of VR users by predicting users' mobility and orientation, as well as determining the user association. To solve this problem, we have developed a novel federated learning algorithm based on echo state networks. The proposed federated ESN algorithm enables the BSs to train their ESN with their locally collected data and share these models to build a global learning model that can predict the entire mobility pattern and orientations of each VR user. To improve the prediction accuracy of the proposed algorithm, we derive a closed-form expression of the memory capacity for ESNs to determine the number of neurons in each ESN model and the values of the recurrent weight matrix. Using these predictions, each BS can determine the user association in both uplink and downlink. Simulation results have shown that the proposed federated ESN approach achieves significant performance gains in terms of BIPs when compared to the centralized ESN and deep learning algorithms.

## APPENDIX

### A. Proof of Theorem 1

Given the input stream vector  $\mathbf{m}_{..t} = [m_1, \dots, m_{t-1}, m_t]$ , the activations  $\mu_{j,t}$  in (10) of the reservoir neuron in ESN model  $l$  at time  $t$  can be given by:

$$\begin{aligned} \mu_{j1,t}^{(l)} = & w_{1,l}^{\text{in}} m_t + w w_{N_W,l}^{\text{in}} m_{t-1} + w^2 w_{N_W-1,l}^{\text{in}} m_{t-2} + \dots + w^{N_W-1} w_{2,l}^{\text{in}} m_{t-(N_W-1)} \\ & + w^{N_W} w_{1,l}^{\text{in}} m_{t-N_W} + w^{N_W+1} w_{N_W,l}^{\text{in}} m_{t-(N_W+1)} + \dots + w^{2N_W-1} w_{2,l}^{\text{in}} m_{t-(2N_W-1)} + w^{2N_W} w_{1,l}^{\text{in}} m_{t-2N_W} \\ & + w^{2N_W+1} w_{N_W,l}^{\text{in}} m_{t-(2N_W+1)} + \dots, \end{aligned} \quad (28)$$

$$\begin{aligned}
\mu_{j2,t}^{(l)} &= w_{2,l}^{\text{in}} m_t + w w_{1,l}^{\text{in}} m_{t-1} + w^2 w_{N_W,l}^{\text{in}} m_{t-2} + \cdots + w^{N_W-1} w_{3,l}^{\text{in}} m_{t-(N_W-1)} \\
&+ w^{N_W} w_{2,l}^{\text{in}} m_{t-N_W} + w^{N_W+1} w_{1,l}^{\text{in}} m_{t-(N+1)} + \cdots + w^{2N_W-1} w_{3,l}^{\text{in}} m_{t-(2N_W-1)} + w^{2N_W} w_{2,l}^{\text{in}} m_{t-2N_W} \\
&+ w^{2N_W+1} w_{1,l}^{\text{in}} m_{t-(2N_W+1)} + \cdots, \\
\mu_{jN_W,t}^{(l)} &\triangleq w_{N_W,l}^{\text{in}} m_t + w w_{N_W-1,l}^{\text{in}} m_{t-1} + w^2 w_{N_W-2,l}^{\text{in}} m_{t-2} + \cdots + w^{N_W-1} w_{1,l}^{\text{in}} m_{t-(N_W-1)} \\
&+ w^{N_W} w_{N_W,l}^{\text{in}} m_{t-N_W} + w^{N_W+1} w_{N_W-1,l}^{\text{in}} m_{t-(N_W+1)} + \cdots + w^{2N_W} w_{N_W,l}^{\text{in}} m_{t-2N_W} \\
&+ w^{2N_W+1} w_{N_W-1,l}^{\text{in}} m_{t-(2N_W+1)} + \cdots,
\end{aligned}$$

where  $w$  is an element of the recurrent matrix  $\mathbf{W}$  which is assumed to be equal for all of the ESN models. The output weight matrix of each ESN model  $l$  can be given by

$$\mathbf{W}_l^{\text{out}} = \mathbf{R}_l^{-1} \mathbf{p}_{k,l},$$

where  $\mathbf{R}_l = \mathbb{E} \left[ \boldsymbol{\mu}_t^{(l)} \left( \boldsymbol{\mu}_t^{(l)} \right)^T \right]$  represents the covariance matrix with  $\boldsymbol{\mu}_t^{(l)} = \left[ \mu_{1,t}^{(l)}, \dots, \mu_{N_W,t}^{(l)} \right]$  and  $\mathbf{p}_{k,l} = \mathbb{E} \left[ \boldsymbol{\mu}_t^{(l)} m_{t-k} \right]$ . The element  $\mathbf{R}_{l,12}$  in  $\mathbf{R}_l$  can be calculated as follows

$$\begin{aligned}
\mathbf{R}_{l,12} &= \mathbb{E} \left[ \mu_{2,t}^{(l)} \mu_{1,t}^{(l)} \right] = \mathbb{E} [w_{1,l}^{\text{in}} w_{2,l}^{\text{in}} m_t^2 + w^2 w_{N_W,l}^{\text{in}} w_{1,l}^{\text{in}} m_{t-1}^2 + \cdots + w^{2(N_W-1)} w_{2,l}^{\text{in}} w_{3,l}^{\text{in}} m_{t-(N_W-1)}^2 \\
&+ w^{2N_W} w_{1,l}^{\text{in}} w_{2,l}^{\text{in}} m_{t-N_W}^2 + \cdots + w^{2(2N_W-1)} w_{2,l}^{\text{in}} w_{3,l}^{\text{in}} m_{t-(2N_W-1)}^2 + w^{4N_W} w_{1,l}^{\text{in}} w_{2,l}^{\text{in}} m_{t-2N_W}^2 + \cdots] \\
&= \sigma^2 (w_{1,l}^{\text{in}} w_{2,l}^{\text{in}} + w^2 w_{N_W,l}^{\text{in}} w_{1,l}^{\text{in}} + \cdots + w^{2(N_W-1)} w_{2,l}^{\text{in}} w_{3,l}^{\text{in}} + w^{2N_W} w_{1,l}^{\text{in}} w_{2,l}^{\text{in}} + w^{2(N_W+1)} w_{N_W,l}^{\text{in}} w_{1,l}^{\text{in}} + \cdots \\
&+ w^{2(2N_W-1)} w_{2,l}^{\text{in}} w_{3,l}^{\text{in}} + w^{4N_W} w_{1,l}^{\text{in}} w_{2,l}^{\text{in}} + \cdots) \\
&= \sigma^2 \sum_{j=0}^{\infty} w^{2N_W j} \left( w_{1,l}^{\text{in}} w_{2,l}^{\text{in}} + w^2 w_{N_W,l}^{\text{in}} w_{1,l}^{\text{in}} + \cdots + w^{2(N_W-1)} w_{2,l}^{\text{in}} w_{3,l}^{\text{in}} \right) \\
&= \frac{\sigma^2}{1 - w^{2N_W}} \left( \text{rot}_1 (\mathbf{w}_{N_W \dots 1,l}^{\text{in}}) \right)^T \Gamma^2 \text{rot}_2 (\mathbf{w}_{N_W \dots 1,l}^{\text{in}}),
\end{aligned} \tag{29}$$

where  $\sigma^2$  is the variance of the input signal  $m_t$ .  $\mathbf{w}_{N_W \dots 1,l}^{\text{in}} = [w_{N_W,l}^{\text{in}}, w_{N_W-1,l}^{\text{in}}, \dots, w_{1,l}^{\text{in}}]$  and  $\text{rot}_k (\mathbf{w}_{N_W \dots 1,l}^{\text{in}})$  denote an operator that rotates vector  $\mathbf{w}_{N_W \dots 1,l}^{\text{in}}$  by  $k$  place to the right. For example,  $\text{rot}_1 (\mathbf{w}_{N_W \dots 1,l}^{\text{in}}) = [w_{1,l}^{\text{in}}, w_{N_W,l}^{\text{in}}, \dots, w_{2,l}^{\text{in}}]$ .  $\Gamma = \text{diag} (1, w, \dots, w^{N_W-1})$ . The element  $\mathbf{R}_{l,ij}$  can be given by

$$\mathbf{R}_{l,ij} = \frac{\sigma^2}{1 - w^{2N_W}} (\text{rot}_i (\mathbf{w}_{N_W \dots 1,l}^{\text{in}}))^T \Gamma^2 \text{rot}_j (\mathbf{w}_{N_W \dots 1,l}^{\text{in}}). \tag{30}$$

Thus,  $\mathbf{R}_l = \frac{\sigma^2}{1 - w^{2N_W}} \mathbf{V}_l^T \Gamma^2 \mathbf{V}_l = \frac{\sigma^2}{1 - w^{2N_W}} \mathbf{A}_l$  where  $\mathbf{A}_l = \mathbf{V}_l^T \Gamma^2 \mathbf{V}_l$ . Similarly, based on (29), element  $p_{k1,l}$  is given by:

$$p_{k1,l} = \mathbb{E} \left[ \mu_{1,t}^{(l)} m_{t-k} \right] = \sigma^2 w^k w_{(N_W-k+1) \bmod N_W,l}^{\text{in}}. \tag{31}$$

We assume that  $w_{0,l}^{\text{in}} = w_{N_W,l}^{\text{in}}$ . Hence,  $\mathbf{p}_{k,l} = \sigma^2 w^k \text{rot}_k(\mathbf{w}_{1\dots N_W,l}^{\text{in}})$ . Then, the output weight matrix of each ESN model  $l$  is  $\mathbf{W}_l^{\text{out}} = (1 - w^{2N_W})w^k \mathbf{A}_l^{-1} \text{rot}_k(\mathbf{w}_{1\dots N_W,l}^{\text{in}})$ .

The output of each ESN model  $l$  at time  $t$  can be given by  $z_{l,t} = (\boldsymbol{\mu}_t^{(l)})^T \mathbf{W}_l^{\text{out}} = (1 - w^{2N_W})w^k (\boldsymbol{\mu}_t^{(l)})^T \mathbf{A}_l^{-1} \text{rot}_k(\mathbf{w}_{1\dots N_W,l}^{\text{in}})$  and  $z_t = \sum_{l=1}^L z_{l,t}$ . Then, the covariance of the output with the  $k$ -slot delayed input can be calculated by:

$$\begin{aligned} \text{Cov}(z_t, m_{t-k}) &= \sum_{l=1}^L (1 - w^{2N_W})w^k \text{Cov}\left(\left(\boldsymbol{\mu}_t^{(l)}\right)^T, m_{t-k}\right) \mathbf{A}_l^{-1} \text{rot}_k(\mathbf{w}_{1\dots N_W,l}^{\text{in}}) \\ &= L(1 - w^{2N_W})w^{2k} \sigma^2 \left(\text{rot}_k(\mathbf{w}_{1\dots N_W,l}^{\text{in}})\right)^T \mathbf{A}_l^{-1} \text{rot}_k(\mathbf{w}_{1\dots N_W,l}^{\text{in}}) \\ &\stackrel{(a)}{=} L(1 - w^{2N_W})w^{2k} \sigma^2 \zeta_k, \end{aligned} \quad (32)$$

where (a) is obtained from the fact that  $\zeta_k = \left(\text{rot}_k(\mathbf{w}_{1\dots N_W,l}^{\text{in}})\right)^T \mathbf{A}_l^{-1} \text{rot}_k(\mathbf{w}_{1\dots N_W,l}^{\text{in}})$ . The variance of the output can be given by:

$$\text{Var}(z_t) = \mathbb{E}\left[\sum_{l=1}^L z_{l,t} \sum_{p=1}^L z_{p,t}\right] - \left(\mathbb{E}\left[\sum_{l=1}^L z_{l,t}\right]\right)^2 = \sum_{l=1}^L \sum_{p=1}^L \mathbb{E}[z_{l,t} z_{p,t}]. \quad (33)$$

Since  $\mathbb{E}\left[\sum_{l=1}^L z_{l,t}\right] = (1 - w^{2N_W})w^{2k} \sigma^2 \zeta_k$ ,  $\text{Var}(z_t) = L^2(1 - w^{2N_W})w^{2k} \sigma^2 \zeta_k$ .

The memory capacity of the parallel ESN model can be given by

$$\begin{aligned} M &= \sum_{k=1}^{\infty} \frac{\text{Cov}^2(m_{t-k}, z_t)}{\text{Var}(m_t) \text{Var}(z_t)} = \frac{1}{L} \sum_{k=0}^{\infty} \frac{\text{Cov}(m_{t-k}, z_t)}{\sigma^2} - \frac{\text{Cov}(m_t, z_t)}{L\sigma^2} \\ &= \frac{1}{L} \sum_{k=0}^{\infty} \sum_{l=1}^L (1 - w^{2N_W})w^{2k} \zeta_k - \frac{1}{L} \sum_{l=1}^L (1 - w^{2N_W})\zeta_0 \\ &= \frac{1}{L} \sum_{l=1}^L (1 - w^{2N_W}) \sum_{k=0}^{\infty} w^{2k} \zeta_k - \frac{1}{L} \sum_{l=1}^L (1 - w^{2N_W})\zeta_0 \\ &= \frac{1}{L} \sum_{l=1}^L (1 - w^{2N_W}) \left[ \sum_{k=0}^{N_W-1} w^{2k} \zeta_k + \sum_{k=N_W}^{2N_W-1} w^{2k} \zeta_k + \dots \right] - \frac{1}{L} \sum_{l=1}^L (1 - w^{2N_W})\zeta_0 \\ &= \frac{1}{L} \sum_{l=1}^L (1 - w^{2N_W}) \left( \sum_{k=0}^{N_W-1} w^{2k} \zeta_k \right) \left( \sum_{k=0}^{\infty} w^{2N_W k} \right) - \frac{1}{L} \sum_{l=1}^L (1 - w^{2N_W})\zeta_0 \\ &= \frac{1}{L} \sum_{l=1}^L \left( \sum_{k=0}^{N_W-1} w^{2k} \zeta_k - (1 - w^{2N_W})\zeta_0 \right) \stackrel{(a)}{=} \frac{1}{L} \sum_{l=1}^L \left( \sum_{k=1}^{N_W-1} w^{2k} \zeta_k + w^{2N_W} \zeta_0 \right) \\ &= \frac{1}{L} \sum_{l=1}^L \left( \sum_{k=1}^{N_W-1} w^{2k} \zeta_k + w^{2N_W} \zeta_{N_W} \right) = \frac{1}{L} \sum_{l=1}^L \left( \sum_{k=1}^{N_W} w^{2k} \zeta_k \right) \stackrel{(b)}{=} N_W - 1 + w^{2N_W}, \end{aligned} \quad (34)$$

where (a) is obtained from the fact that  $\zeta_0 = \zeta_{N_W}$  and (b) stems from the fact that  $w_l^{2k} \zeta_k = 1$  as  $k = 1, \dots, N_W - 1$  and  $w^{2N_W} \zeta_{N_W} = w^{2N_W}$ . This completes the proof.

### B. Proof of Theorem 2

Let  $\mathbf{m}_{\dots t} = [m_1, \dots, m_{t-1}, m_t]$  be the input steam vector and  $z_t^{(l)}$  be the output of ESN model  $l$ . Next, we derive the memory capacity of a series ESN model using an enumeration method. First, according to (28)-(33), we have  $\text{Cov}(z_t^{(1)}, m_{t-k}) = (1 - w^{2N_W}) w^{2k} \sigma^2 \zeta_k$ . Given the output of the first ESN model,  $z_t^{(1)}$ , which is the input of the second ESN model, then  $\text{Cov}(z_t^{(2)}, m_{t-k}) = (1 - w^{2N_W})^2 w^{2k} \zeta_k \sigma^2$ . Similarly, we can obtain that  $\text{Cov}(z_t^{(3)}, m_{t-k}) = (1 - w^{2N_W})^3 w^{2k} \zeta_k \sigma^2$ . Therefore, we can conclude that  $\text{Cov}(z_t^{(L)}, m_{t-k}) = (1 - w^{2N_W})^L w^{2k} \zeta_k$ . Based on (35), the memory capacity of a series ESN can be given by  $\sum_{k=0}^{\infty} (1 - w^{2N_W})^L w^{2k} \zeta_k - (1 - w^{2N_W})^L \zeta_0$ . Then, the memory capacity of a series ESN is

$$\begin{aligned}
 M &= \sum_{k=0}^{\infty} (1 - w^{2N_W})^L w^{2k} \zeta_k - (1 - w^{2N_W})^L \zeta_0 = (1 - w^{2N_W})^L \sum_{k=0}^{\infty} w^{2k} \zeta_k - (1 - w^{2N_W})^L \zeta_0 \\
 &= (1 - w^{2N_W})^L \left[ \sum_{k=0}^{N_W-1} w^{2k} \zeta_k + \sum_{k=N_W}^{2N_W-1} w^{2k} \zeta_k + \dots \right] - (1 - w^{2N_W})^L \zeta_0 \\
 &= (1 - w^{2N_W})^L \left( \sum_{k=0}^{N_W-1} w^{2k} \zeta_k \right) \left( \sum_{k=0}^{\infty} w^{2N_W k} \right) - (1 - w^{2N_W})^L \zeta_0 \\
 &= (1 - w^{2N_W})^L \left( \frac{\sum_{k=0}^{N_W-1} (w^{2k} \zeta_k)^L}{1 - w^{2N_W}} - \frac{\zeta_0 - \zeta_0 w^{2N_W}}{1 - w^{2N_W}} \right) \\
 &= (1 - w^{2N_W})^{L-1} (N_W - 1 + w^{2N_W}).
 \end{aligned} \tag{35}$$

This completes the proof.

### C. Proof of Theorem 3

The memory capacity of a single ESN with multiple inputs is derived using an enumeration method. Consider  $K = 2$ , then the input stream will be  $\mathbf{m}_{\dots t} = [\mathbf{m}_{\dots 1t}, \mathbf{m}_{\dots 2t}]$  where  $\mathbf{m}_{\dots kt} = m_{k1} \dots m_{kt-2} m_{kt-1} m_{kt}$ . Based on the proof of Theorems 1 and 2,  $\mathbf{R}$  can be given by:

$$\mathbf{R} = \frac{\sigma_1^2 + 2\rho_{12}\sigma_1\sigma_2 + \sigma_2^2}{1 - w^{2N_W}} \mathbf{V}^T \Gamma^2 \mathbf{V} = \frac{\sigma_1^2 + 2\rho_{12}\sigma_1\sigma_2 + \sigma_2^2}{1 - w^{2N_W}} \mathbf{A}, \tag{36}$$

and  $\mathbf{p}_k = w^k (\sigma_1^2 + \sigma_2^2) \text{rot}_k(\mathbf{V}_{1\dots N})$ . Then the output weight matrix can be given by:

$$\mathbf{W}^{\text{out}} = (1 - w^{2N_W}) w^k \frac{\sigma_1^2 + \sigma_2^2}{\sigma_1^2 + 2\rho_{12}\sigma_1\sigma_2 + \sigma_2^2} \mathbf{A}^{-1} \text{rot}_k(\mathbf{V}_{1\dots N}). \tag{37}$$

The output at time  $t$  is

$$z_t = (\mathbf{m}_t)^T \mathbf{W}^{\text{out}} = (1 - w^{2N_W}) w^k \frac{\sigma_1^2 + \sigma_2^2}{\sigma_1^2 + 2\rho_{12}\sigma_1\sigma_2 + \sigma_2^2} (\mathbf{m}_t)^T \mathbf{A}^{-1} \text{rot}_k (\mathbf{V}_{1\dots N}). \quad (38)$$

The covariance of the output at time  $t$  and  $t - k$  can be given by:

$$\begin{aligned} \text{Cov}(z_t, \mathbf{m}_{t-k}) &= (1 - w^{2N_W}) w^k \frac{\sigma_1^2 + \sigma_2^2}{\sigma_1^2 + 2\rho_{12}\sigma_1\sigma_2 + \sigma_2^2} \text{Cov}\left((\boldsymbol{\mu}_t)^T, \mathbf{m}_{t-k}\right) \times \mathbf{A}^{-1} \text{rot}_k (\mathbf{V}_{1\dots N}) \\ &= (1 - w^{2N_W}) w^{2k} \frac{(\sigma_1^2 + \sigma_2^2)^2}{\sigma_1^2 + 2\rho_{12}\sigma_1\sigma_2 + \sigma_2^2} \zeta_k. \end{aligned}$$

Based on (33),  $\text{Var}(z_t) = \text{Cov}(z_t, \mathbf{m}_{t-k})$ . Then, the memory capacity can be given by

$$\begin{aligned} M &= \sum_{k=0}^{\infty} \frac{\text{Cov}^2(z_t, \mathbf{m}_{t-k})}{\text{Var}(\mathbf{m}_{t-k}) \text{Var}(z_t)} - \frac{\text{Cov}^2(z_t, \mathbf{m}_t)}{\text{Var}(\mathbf{m}_t) \text{Var}(z_t)} = \sum_{k=0}^{\infty} \frac{\text{Cov}(z_t, \mathbf{m}_{t-k})}{\sigma_1^2 + 2\rho_{12}\sigma_1\sigma_2 + \sigma_2^2} - \frac{\text{Cov}(z_t, \mathbf{m}_t)}{\sigma_1^2 + 2\rho_{12}\sigma_1\sigma_2 + \sigma_2^2} \\ &= \left( \frac{\sigma_1^2 + \sigma_2^2}{\sigma_1^2 + 2\rho_{12}\sigma_1\sigma_2 + \sigma_2^2} \right)^2 \times (1 - w^{2N_W}) \sum_{k=0}^{N_W-1} w^{2k} \zeta_k \sum_{j=0}^{\infty} r^{2N_W j} - (1 - w^{2N_W}) \\ &= \left( \frac{\sigma_1^2 + \sigma_2^2}{\sigma_1^2 + 2\rho_{12}\sigma_1\sigma_2 + \sigma_2^2} \right)^2 \sum_{k=0}^{N_W-1} w^{2k} \zeta_k - (1 - w^{2N_W}) = \left( \frac{\sigma_1^2 + \sigma_2^2}{\sigma_1^2 + 2\rho_{12}\sigma_1\sigma_2 + \sigma_2^2} \right)^2 (N_W - 1 + w^{2N_W}). \end{aligned} \quad (39)$$

Similarly, we can formulate the memory capacity of the single ESN with input vector  $\mathbf{m}_t = [\mathbf{m}_{1t}, \mathbf{m}_{2t}, \mathbf{m}_{3t}]$ , which is given by  $\left( \frac{\sigma_1^2 + \sigma_2^2 + \sigma_3^2}{\sigma_1^2 + 2\rho_{12}\sigma_1\sigma_2 + 2\rho_{13}\sigma_1\sigma_3 + 2\rho_{23}\sigma_2\sigma_3 + \sigma_2^2 + \sigma_3^2} \right)^2 (N_W - 1 + w^{2N_W})$ .

In consequence, the memory capacity of a single ESN with input vector  $\mathbf{m}_t = [\mathbf{m}_{1t}, \dots, \mathbf{m}_{Kt}]$  can be given by  $\left( \frac{\sum_{l=1}^K \sigma_l^2}{\sum_{k=1}^K \sum_{n=1}^K \rho_{kn} \sigma_k \sigma_n} \right)^2 (N_W - 1 + w^{2N_W})$ . This completes the proof.

#### D. Proof of Theorem 4

For uplink user association, each VR user  $i$  needs to only find a BS that can minimize the time used for tracking information transmission from VR user  $i$  to BS. Hence, for user  $i$ , the BS that can minimize the uplink transmission delay is given by  $\arg \min_{a_{ij,t}^{\text{UL}}} \frac{A}{a_{ij,t}^{\text{UL}} c_{ij}^{\text{UL}}(\hat{x}_{it}, \hat{y}_{it})}$ . For downlink user association, each VR user  $i$  needs to find a BS that can guarantee the transmission delay and VR video quality. Since we have determined the user association over uplink, the maximum time used for VR video transmission can be given by  $\gamma_D - \frac{A}{a_{i*,t}^{\text{UL}} c_{i*}^{\text{UL}}(\hat{x}_{it}, \hat{y}_{it})}$ . Consequently, user  $i$  needs to connect with a BS that can satisfy the transmission delay requirement of user  $i$ , i.e.,  $\frac{D(\mathbf{l}_{i,t}(a_{ik,t}^{\text{DL}} c_{ik}^{\text{DL}}(\hat{x}_{it}, \hat{y}_{it}, b_i(\hat{x}_{it}), n_{ik})))}{a_{ik,t}^{\text{DL}} c_{ik}^{\text{DL}}(\hat{x}_{it}, \hat{y}_{it}, b_i(\hat{x}_{it}), n_{ik})} \leq \gamma_D - \frac{A}{a_{i*,t}^{\text{UL}} c_{i*}^{\text{UL}}(\hat{x}_{it}, \hat{y}_{it})}$ . Moreover, user  $i$  needs to associate with a BS that can meet the requirement of VR video quality, i.e.,  $\mathbf{l}_{i,t}(a_{ik,t}^{\text{DL}} c_{ik}^{\text{DL}}(\hat{x}_{it}, \hat{y}_{it}, b_i(\hat{x}_{it}), n_{ik})) \mathbf{m}_{i,t}(G_A) \geq \gamma_Q$ . Thus, if BS  $k$  can satisfy the following conditions:  $\frac{D(\mathbf{l}_{i,t}(a_{ik,t}^{\text{DL}} c_{ik}^{\text{DL}}(\hat{x}_{it}, \hat{y}_{it}, b_i(\hat{x}_{it}), n_{ik})))}{a_{ik,t}^{\text{DL}} c_{ik}^{\text{DL}}(\hat{x}_{it}, \hat{y}_{it}, b_i(\hat{x}_{it}), n_{ik})} \leq \gamma_D -$



$\frac{A}{a_{i*,t}^{UL} c_{i*,t}^{UL}(\hat{x}_{it}, \hat{y}_{it})}$  and  $\mathbf{l}_{i,t}(a_{ik,t}^{DL} c_{ik,t}^{DL}(\hat{x}_{it}, \hat{y}_{it}, b_i(\hat{x}_{it}), n_{ik})) \mathbf{m}_{i,t}(G_A) \geq \gamma_Q$ , user  $i$  can associate with it. This completes the proof.

## REFERENCES

- [1] E. Baştuğ, M. Bennis, M. Médard, and M. Debbah, “Towards interconnected virtual reality: Opportunities, challenges and enablers,” *IEEE Communications Magazine*, vol. 55, no. 6, pp. 110–117, Jan. 2017.
- [2] O. Semiari, W. Saad, M. Bennis, and M. Debbah, “Integrated millimeter wave and sub-6 GHz wireless networks: A roadmap for joint mobile broadband and ultra-reliable low-latency communications,” *IEEE Wireless Communications Magazine*, to appear, 2018.
- [3] Y. Sun, Z. Chen, M. Tao, and H. Liu, “Communication, computing and caching for mobile VR delivery: Modeling and trade-off,” *arXiv preprint arXiv:1804.10335*, April 2018.
- [4] J. Park and M. Bennis, “URLLC-eMBB slicing to support VR multimodal perceptions over wireless cellular systems,” *available online: arxiv.org/abs/1805.00142*, May 2018.
- [5] X. Yang, Z. Chen, K. Li, Y. Sun, N. Liu, W. Xie, and Y. Zhao, “Communication-constrained mobile edge computing systems for wireless virtual reality: Scheduling and tradeoff,” *IEEE Access*, vol. 6, pp. 16665–16677, March 2018.
- [6] A. Taleb Zadeh Kasgari, W. Saad, and M. Debbah, “Human-in-the-loop wireless communications: Machine learning and brain-aware resource management,” *arXiv preprint arXiv:1804.00209*, March 2018.
- [7] M. S. Elbamby, C. Perfecto, M. Bennis, and K. Doppler, “Edge computing meets millimeter-wave enabled VR: Paving the way to cutting the cord,” in *Proc. of IEEE Wireless Communications and Networking Conference*, Barcelona, Spain, April 2018.
- [8] W. C. Lo, C. L. Fan, S. C. Yen, and C. H. Hsu, “Performance measurements of 360 video streaming to head-mounted displays over live 4G cellular networks,” in *Proc. of Asia-Pacific Network Operations and Management Symposium*, Seoul, South Korea, Sept 2017.
- [9] M. Chen, W. Saad, and C. Yin, “Virtual reality over wireless networks: Quality-of-service model and learning-based resource management,” *IEEE Transactions on Communications*, vol. 66, no. 11, pp. 5621–5635, Nov. 2018.
- [10] J. Yin, L. Li, H. Zhang, X. Li, A. Gao, and Z. Han, “A prediction-based coordination caching scheme for content centric networking,” in *Proc. of Wireless and Optical Communication Conference*, Hualien, Taiwan, April 2018.
- [11] H. Lee, M. Wicke, B. Kusy, O. Gnawali, and L. Guibas, “Predictive data delivery to mobile users through mobility learning in wireless sensor networks,” *IEEE Transactions on Vehicular Technology*, vol. 64, no. 12, pp. 5831–5849, Dec 2015.
- [12] L. Yao, A. Chen, J. Deng, J. Wang, and G. Wu, “A cooperative caching scheme based on mobility prediction in vehicular content centric networks,” *IEEE Transactions on Vehicular Technology*, vol. 67, no. 6, pp. 5435–5444, June 2018.
- [13] N. T. Nguyen, Y. Wang, H. Li, X. Liu, and Z. Han, “Extracting typical users’ moving patterns using deep learning,” in *Proc. of IEEE Global Communications Conference*, Anaheim, CA, USA, Dec 2012.
- [14] M. Chen, M. Mozaffari, W. Saad, C. Yin, M. Debbah, and C. S. Hong, “Caching in the sky: Proactive deployment of cache-enabled unmanned aerial vehicles for optimized quality-of-experience,” *IEEE Journal on Selected Areas on Communications (JSAC)*, vol. 35, no. 5, pp. 1046–1061, May 2017.
- [15] O. Esrafilian, R. Gangula, and D. Gesbert, “Learning to communicate in UAV-aided wireless networks: Map-based approaches,” *IEEE Internet of Things Journal*, to appear, 2018.
- [16] P. de Kerret and D. Gesbert, “Robust decentralized joint precoding using team deep neural network,” in *2018 15th International Symposium on Wireless Communication Systems (ISWCS)*, Lisbon, Portugal, Aug 2018.
- [17] M. Chen, U. Challita, W. Saad, C. Yin, and M. Debbah, “Machine learning for wireless networks with artificial intelligence: A tutorial on neural networks,” *available online: arxiv.org/abs/1710.02913*, Oct. 2017.
- [18] O. Semiari, W. Saad, and M. Bennis, “Joint millimeter wave and microwave resources allocation in cellular networks with dual-mode base stations,” *IEEE Transactions on Wireless Communications*, vol. 16, no. 7, pp. 4802–4816, July 2017.
- [19] HTC, “HTC vive,” <https://www.vive.com/us/>.
- [20] Oculus, “Mobile VR media overview,” <https://www.oculus.com/>.
- [21] O. Semiari, W. Saad, M. Bennis, and Z. Dawy, “Inter-operator resource management for millimeter wave multi-hop backhaul networks,” *IEEE Transactions on Wireless Communications*, vol. 16, no. 8, pp. 5258–5272, Aug 2017.
- [22] J. Jerald, *The VR book: Human-centered design for virtual reality*, Morgan & Claypool, Sept. 2015.
- [23] J. Chung, H. J. Yoon, and H. J. Gardner, “Analysis of break in presence during game play using a linear mixed model,” *ETRI journal*, vol. 32, no. 5, pp. 687–694, Oct. 2010.
- [24] M. M. Amiri and D. Gunduz, “Computation scheduling for distributed machine learning with straggling workers,” *arXiv preprint arXiv:1810.09992*, Oct. 2018.
- [25] V. Smith, C. K. Chiang, M. Sanjabi, and A. S. Talwalkar, “Federated multi-task learning,” in *Proc. of Advances in Neural Information Processing Systems*, Long beach, CA, USA, Dec. 2017.
- [26] M. Chen, W. Saad, C. Yin, and M. Debbah, “Echo state networks for proactive caching in cloud-based radio access networks with mobile users,” *IEEE Transactions on Wireless Communications*, vol. 16, no. 6, pp. 3520–3535, June 2017.
- [27] M. Bennis and D. Niyato, “A Q-learning based approach to interference avoidance in self-organized femtocell networks,” in *Proc. of IEEE Global Communications Conference Workshops*, Miami, FL, USA, Dec 2010.